# STUDY OF CARBONATE AGGREGATE PORE SYSTEMS BY IMAGE ANALYSIS

by

Gregg Garychuk

A thesis
presented to the University of Manitoba
in partial fulfillment of the
requirements for the degree of
MASTER OF SCIENCE IN CIVIL ENGINEERING
in
THE DEPARTMENT OF CIVIL ENGINEERING

Winnipeg, Manitoba

ISBN 0-315-44186-0

# STUDY OF CARBONATE AGGREGATE PORE SYSTEMS BY IMAGE ANALYSIS

BY

GREGG GARYCHUK

A thesis submitted to the Faculty of Graduate Studies of
the University of Manitoba in partial fulfillment of the requirements
of the degree of

MASTER OF SCIENCE

The University of Manitoba requires the signatures of all persons using or photocopying this thesis. Please sign below, and give address and date.

I hereby declare that I am the sole author of this thesis.

I authorize the University of Manitoba to lend this thesis to other institutions or individuals for the purpose of scholarly research.

Gregg William Garychuk

I further authorize the University of Manitoba to reproduce this thesis by photocopying or by other means, in total or in part, at the request of other institutions or individuals for the purpose of scholarly research.

Gregg William Garychuk

**ABSTRACT**

D-cracking is a phenomenon that has been attributed to the freeze-thaw deterioration of certain carbonate rock porosity types. The economic implications of this manifestation on local portland cement concrete pavements using these aggregates has mandated the development of improved aggregate assessment techniques.

Petrographic Image Analysis (PIA) is a technique that combines computer based image processing with two dimensional microscopic analysis of carbonate pore space. This procedure attempts to characterize the geometry of the pore complex using separate spectra related to the pore-size and pore-roughness of each sample.

The purpose of this thesis was to evaluate the relevance of PIA techniques to the assessment of local D-cracking susceptible aggregate sources. Twenty-six specimens were analyzed on a LEITZ TAS PLUS image analyzer using a simplified 'Pore-Complex Spectra' algorithm. Total Optical Porosity (TOP) ranged from 15.1% to 23.4% for the non-durable specimens and from 5.2% to 22.4% for the durable specimens. The test data indicated that a direct relationship between PIA parameters and the D-cracking susceptibility of carbonate aggregates may exist.

**ACKNOWLEDGEMENTS**

The author wishes to extend sincere gratitude to his advisor, Dr. L. Domaschuk for his guidance and support throughout the project.

Special thanks is extended to Kim Mysyk for his petrographic expertise and helpful discussions.

The assistance provided by Chief Technician Ed Lemke, for the design and fabrication of sample preparation apparatus, is acknowledged. Thanks is also granted to Research Technician Don Mardis for assistance in sample preparation and computer operation.

Appreciation is extended to William Sheftick and the Illinois Department of Transport(DOT) for providing the study with several carbonate rock samples.

Special thanks is extended to Dr. R. Ehrlich and Phd. student Jack Horkowitz of the University of South Carolina for their invaluable information on image analysis theory and for the computer techniques which they provided.

The patience, support and understanding provided by Jaqueline Halcrow during the writing of this paper is warmly appreciated.

Financial assistance throughout the program, provided in the form of a Postgraduate Scholarship from NSERC and research grants from Transport Canada and The Transportation Institute, is acknowledged.

Leaf inserted to correct page numbering.

CONTENTS

## LIST OF TABLES

## LIST OF FIGURES

# Chapter I

## INTRODUCTION

D-cracking has been defined as "fine cracking in a concrete slab surface in a pattern that appears first in an orientation parallel to transverse and longitudinal joints and cracks, continues around corners and may progress towards the center"(Girard et.al. 1982). This phenomenon is attributed to freeze-thaw deterioration of the coarse carbonate aggregate fraction in portland cement concrete and is found to occur almost exclusively in certain types of carbonate aggregates. Such deterioration has lead to the severe debilitation of concrete pavements long before the projected design life. Methods for the evaluation of aggregate durability for use in portland cement concrete pavements that are exposed to freeze-thaw and wet-dry cycles have been the subject of many research programs.

The purpose of this study was to review various techniques of pore structure analysis of porous media relevant to the study of carbonate rock aggregates susceptible to D-cracking. The pore-structure includes the volume of pores (porosity), their surface area, pore-size distribution and shape and spatial distribution parameters (Zagar 1973). Pore system characteristics are important because of their

direct influence on the physical and chemical properties of the pores which govern the flow of moisture in and out of an aggregate, the water retentivity and the development of pressure during freeze-thaw cycles (Hiltrop et.al. 1960). Misinterpretation of the mechanisms involved in freeze-thaw deterioration has led to the development of many empirical test procedures which are often misleading. The parameters measured in these standard tests are a function of the pore structure but may not be directly related to the freeze-thaw durability of the aggregate. The durability of carbonate aggregates subject to temperature and moisture fluctuations are though to be related in some fundamental way to the pore-structure.

A general review of carbonate pore-structure is presented to introduce the types, shapes, sizes and order of magnitude of the porosity under investigation. Important aspects of the physical characteristics that define carbonate pore systems are introduced. The ultimate strength of carbonate aggregates, that is directly influenced by the pore structure, is discussed in terms of mineralogical composition.

Currently accepted theories, proposed to describe the basic mechanisms of frost action in porous systems are also reviewed. Various characteristic features of frost action in porous media are introduced and their importance to freeze-thaw deterioration of carbonate aggregates is discussed.

Laboratory tests and techniques used for the determination of aggregate pore-structure and pore-structure related properties are presented from two different perspectives. The first perspective, referred to as geotechnical test methods, was developed specifically for the evaluation of freeze-thaw durability of concrete aggregates. These tests have been separated into two catagories; 1)tests based on environmental simulation 2)tests based on aggregate properties correlated to field performance. These test procedures are defined and their relationship to pore-structure analysis is discussed. The second group referred to as geological test methods have primarily been used to evaluate carbonate porosity for reservoir potential. These test methods are reviewed and their importance to pore-structure analysis is discussed.

The final section of the literature review deals with computer techniques collectively referred to as image analysis. Image analysis is a facet of stereology that quantitatively evaluates the statistical and geometrical properties of 2-dimensional images. In this study these planar images are a representation of the aggregate mineral grain or pore structure. Basic image analysis system operation and common stereometric parameters, features and characteristics used for porosity analysis are discussed. Various image analysis procedures including Petrographic Image Analysis (PIA) techniques for image processing and data aquisition

are presented and discussed. Several other basic pore-structure analysis procedures and interpretations are introduced and comparisons with standard tests evaluated.

In the laboratory investigation the basic petrographic analysis techniques for micro-porosity analysis of carbonate rock aggregates are discussed. Several different aggregates of varying freeze-thaw durablity were analyzed to assess the viability of using a LEITZ TAS PLUS image analyzer for the investigation of carbonate porosity relevant to the study of D-cracking.

Sample description techniques including X-ray diffraction and SEM microscopy accompanied by a petrographic description are presented and discussed.

Samples were prepared using a technique known as pore casting, followed by grinding and polishing to produce a 2-dimensional image of a plane passing through the porous media. Veiwed under a microscope these images were then quantitatively analyzed using the image analysis computer.

# Chapter II

# LITERATURE REVIEW

## 2.1 CARBONATE POROSITY

The pores and pore systems of sedimentary carbonates are normally complex both physically and genetically. Carbonate sedimentary rocks ranging in composition from pure limestone to dolomite (some with varying amounts of clay and/or chert) have been identified as frost susceptible (Stark 1976). Recent attempts have been made to quantitatively analyze the geometry of pore openings, their shape, size, distribution and orientation.

The complexity of the size and shape of pores in carbonate rocks is caused by many factors. The energy of the depositional environment dictates the size of the particles and the nature of the porosity. It relates partly to the wide range in shape and size of the sedimentary carbonate particles which create pores by packing or solution. In most carbonates, most of the original pore space created during primary deposition is altered physically, chemically and biologically by a process called diagenesis. Diagenesis is a process of porosity evolution, where new pore-structures are formed within identifiable stratographic

zones. The pore-structure is altered over geological time through processes of solution and dissolution. Dolimitization, a solution process, is the conversion of limestone to dolomite. This process results in an increase of porosity due to recrystalization of calcite to dolomite. The continued growth of dolomite crystals reduces the porosity as polyhedral pores and finally interboundary sheet pores (ISP) are formed. This reduction in porosity results in a simpler and more regular pore geometry and also increases the pore-size to pore throat-size ratio (Wardlaw 1976). Pores are not simply voids but they signify the occurrence of a fluid or gaseous phase. A pore/porewall interface possesses surface energy exactly like other mineralogical interfaces (Ehrlich et. al. 1984).

There are fifteen recognized basic types of porosity, eight of which are extremely common and volumetrically important. This porosity forms the three-dimensionally interconnected pore network of sedimentary carbonate formations. Conventionally, wider parts of the network are termed pores and narrower parts pore throats. Geological nomenclature and classification of porosity gives concise description for the interpretation of porosity in sedimentary carbonates (Choquette and Pray 1970). Figure 1 illustrates the basic porosity types and gives the modifying terms for an accurate geological description.

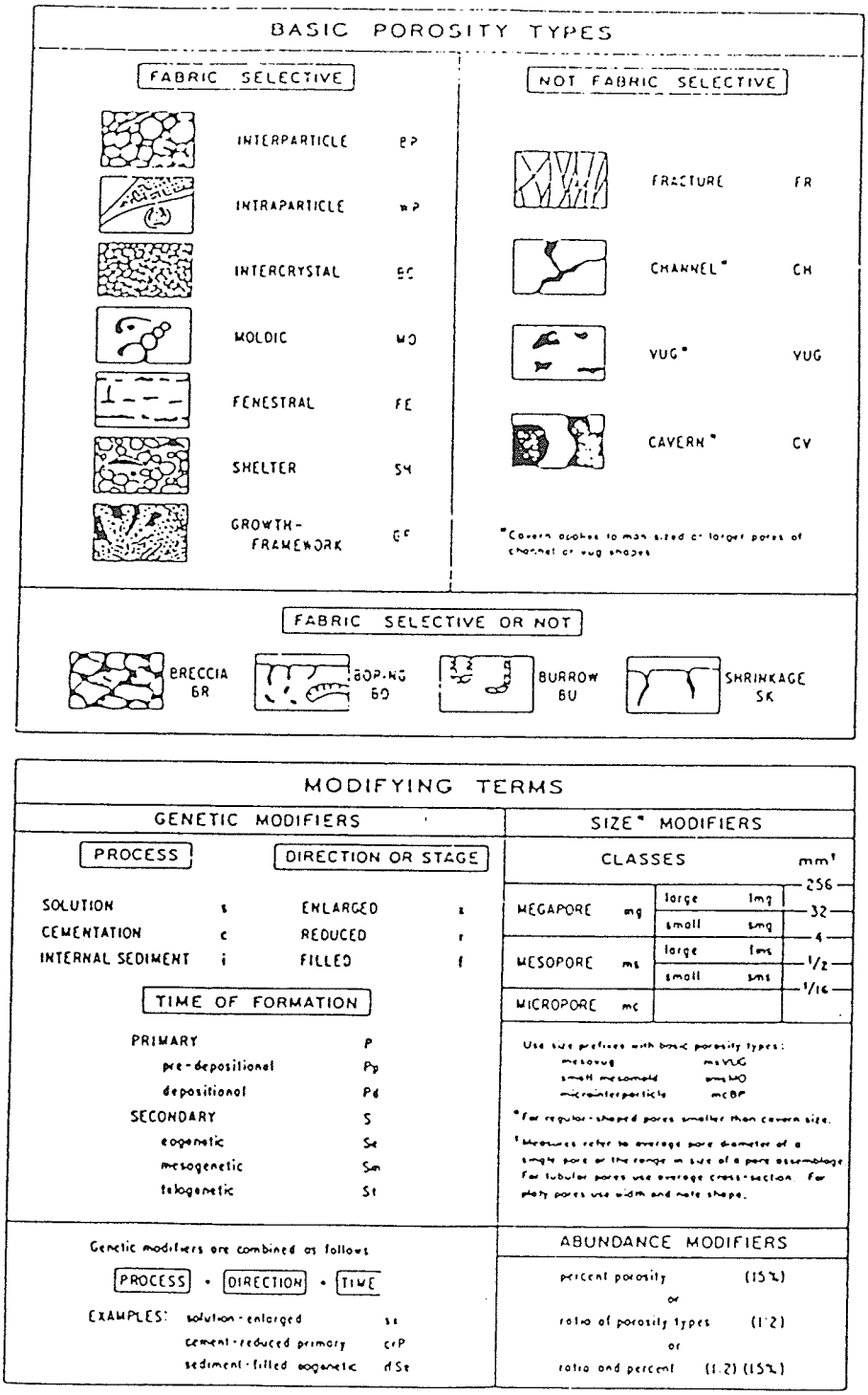


Figure 1: Geological classification of pores and pore systems in carbonate rocks (Choquette and Pray 1970)

Traditionally there have been two classifications of porosity, primary and secondary porosity. Primary porosity is referred to as all pore space present after final deposition. Secondary porosity is any porosity created after final deposition. Table 1 describes the major types of porosity and relates the processes of formation to the permeability (Mysyk et. al. 1985).

For basic pore-structure analysis a gradation scale is required to identify the size of regular shaped pores, utilizing the average diameter of equant or tubular pores or the width of platy pores. The grain size scale for carbonate rocks (Figure 2) satisfies general petrographic description but gives little useful information relevant to the microstructure of the pore system. A Geological gradation scale was propsed by Choquette and Pray (1970) for preliminary identification of microscopic description of carbonate rocks (Table 2). A different gradation scale (Table 3) used in adsorption studies was developed for the microstructure analysis of porous media which divides pore-size into micropores, mesopores (transitional pores) and macropores (Brunauer et.al. 1973).

The principle characteristics of pore systems must be described by well defined, physical characteristics related to the properties and processes considered. The principle indices of a pore system are (Valenta 1973):

-total porosity

# TABLE 1

## Major types of porosity (Mysyk and Edwards 1985)

MAJOR TYPES OF POROSITY*

I. Primary

| Type | Description | Process of Formation | Effect on Permeability | |
|---|---|---|---|---|
| 1. Intergranular or Interparticle | Porosity between grains and/or particles. | Forms during final sedimentation of detrital particles. May also form by leaching of matrix or cement. Either type may be increased by later dissolution processes or dolomitization; the general term applied for this is "Enhanced" primary porosity. | Permeability controlled largely by pore shape and size, which is in turn controlled partly by grain size and shape. | Both types may be enhanced by dissolution around the original pores. |
| 2. Intragranular | Porosity within individual particles or grains | | Least important, contributes little to permeability. | |

II. Primary or Secondary

| | | | |
|---|---|---|---|
| 3. Intercrystal | Porosity between crystals of relatively similar size that have grown in place, e.g. sucrosic dolomite | Forms during final sedimentation stage of chemically precipitated carbonate crystals. May also form by leaching of matrix or cement. | Permeability strongly controlled by size of pores which is generally controlled by the crystal size: the finer the grains, the lower the permeability. |

III. Secondary

| | | | |
|---|---|---|---|
| 4. Vuggy | Irregular, usually secondary holes in a rock that cut across grain and/or cement boundaries | Formed by nonselective dissolution. | Permeability strongly controlled by size and number of connections getween molds (vugs). Low permeability results if the molds (vugs) are isolated by cement or matrix with low intercrystalline porosity. |
| 5. Moldic | Implies what was occupying the vug (i.e. fossilmoldic, oolmoldic) | Formed by selective dissolution of less resistant grains (e.g. aragonite). | |
| 6. Fracture | Fissures or cracks in the rock characterized by little relative displacement of adjacent blocks. | Formed by fracturing that may be associated with folding, faulting, salt solution or fluid overpressuring. Usually independent of primary porosity. | Generally high permeability, low porosity. |
| 7. Breccia | More severe version of fracture porosity where blocks are jumbled and chaotic. | Formed by tectonic processes, salt solution and collapse, or rapid, chaotic sedimentation. Totally independent of primary porosity (not fabric related). | Generally high permeability, low porosity. |
| 8. Stylolitic | A thin seam marked by an irregular and interlocking of two bedding surfaces, characterized by a concentration of insoluble residue (clay, carbon, sand, iron oxides) | Diagenetic feature formed by differential vertical movement under pressure, accompanied by solution. | May have high permeability (if open) but low porosity. |

Compiled from Choquette and Pray, 1970; Asquith, 1979; Longman, 1981.

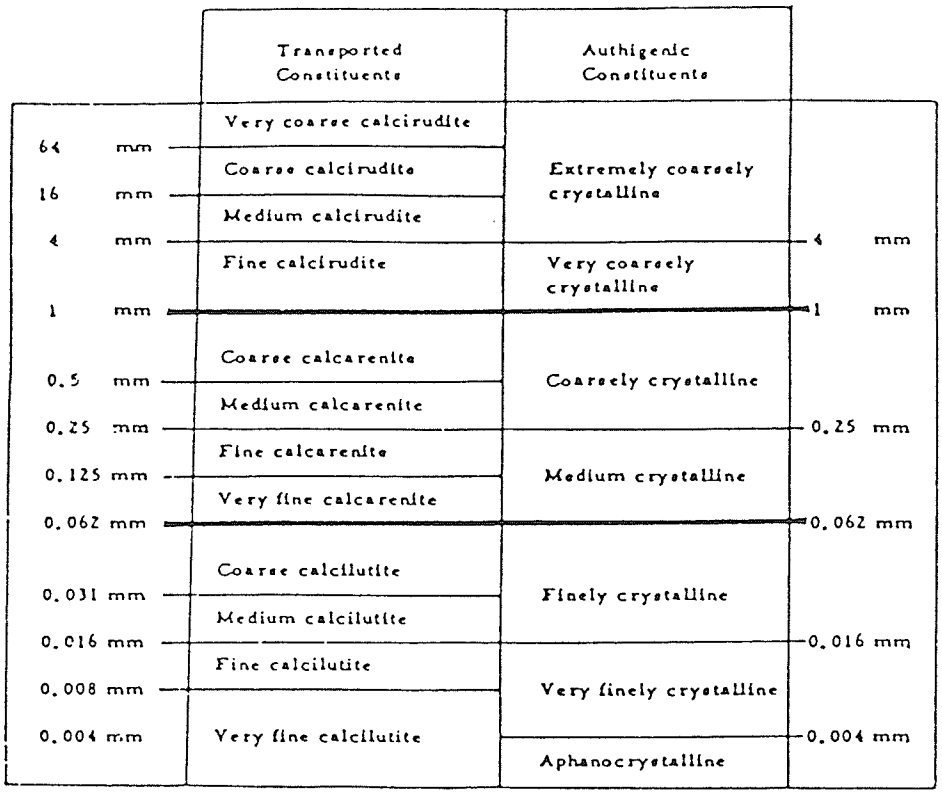


Figure 2: Grain-size scale for carbonate rocks (Folk 1962)

-effective porosity

-size of pores

-shape of pores

-extent and nature of channels of various size, shape, x-section and arrangement

-distribution (pore-size, spatial)

-spacing and uniformity

-orientation

TABLE 2

Geological gradation scale (Choquette and Pray 1970)

| | | | |
|---|---|---|---|
| micropores | < | 1/16 mm | |
| mesopores | - | 1/16 - 4 mm | small<br>large |
| macropores | - | 4 - 256 mm | small<br>large |

TABLE 3

Adsorption study gradation scale (Brunaer et. al. 1973)

| | | |
|---|---|---|
| micropores | < | 16 A° |
| mesopores | - | 16 - 1000 A° |
| macropores | > | 1000 A° |

Conversions

1 A - $10^{-10}$ m

1 μ - $10^{-6}$ m

1 μ - 10,000 A

1 mm - 1,000 μ

Petroleum recovery investigations using artificial and theoretical pore network models (Wardlaw 1976,1981) suggested that the important aspects of pore systems were; pore to pore throat ratio, throat to pore coordination number or connectivity and the types and extent of random and non-random heterogeneities of the system.

The coarse carbonate aggregates identified as frost susceptible have been reported to have a pore-size range between 0.04-0.02 microns (Stark 1976). Tests using ceramic samples of different porosities implied that a high percentage of pores between 0.25-1.4 microns results in poor frost susceptibility (Ravaglioli 1973). Research in frost action in porous systems concluded that pores with radii in the range of 0.3-0.04 microns can cause frost damage most often (Litvan 1973).

## 2.2 CARBONATE STRENGTH

Hugman and Friedman conducted tests on dry, low-porosity rocks with a wide range of texture and dolomite content. These samples were experimentally deformed at room temperature using a strain rate of $.00001^{-1}$ sec and confining pressures of 0, 50, and 100 MPa to evaluate the effects of texture and composition on ultimate strength in low porosity carbonate rocks (Hugman and Friedman 1979). Grain size was found to be the dominant intrinsic rock property that affects the ultimate strength in low porosity carbonate rocks.

The weighted mean grain size and microcrystalline carbonate (micrite) content, determined by petrographic microscope point count, were found to have the highest linear correlation with ultimate strength. Ultimate strength was found to increase with increasing dolomite content, determined by X-ray diffraction, in similarly textured rocks. This was not necessarily true in differently textured rocks. Pure dolomites are generally stronger and more brittle than limestones. Limestones and dolomites composed entirely of microcrystalline carbonate are stronger and more brittle than coarse grained carbonates. Dolomite and microcrystalline carbonate contents were found to be the most important factors governing ultimate strength (Figure 3).

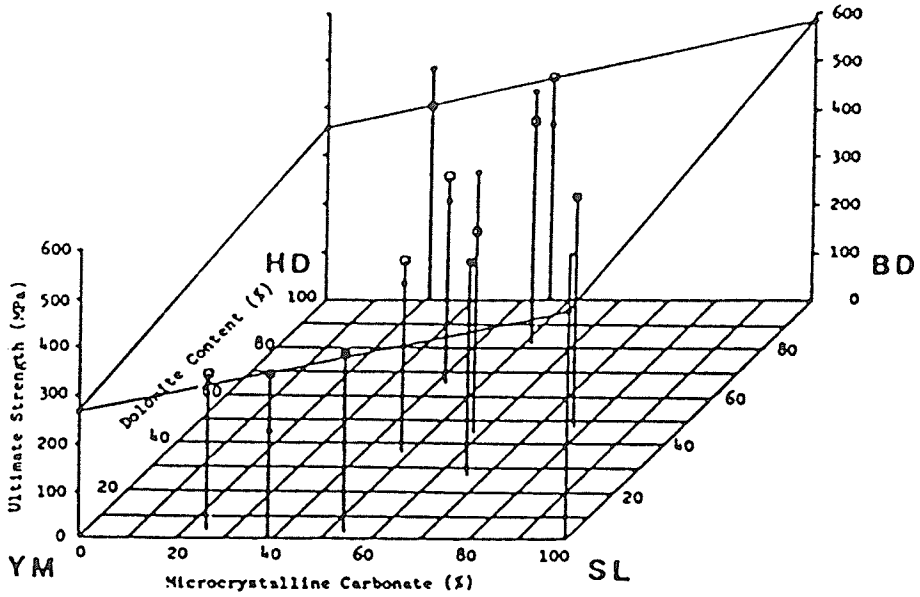


Figure 3: Ultimate strength as a function of dolomite and microcrystalline carbonate contents (Hugman and Friedman 1979)

## 2.3 BASIC MECHANISM OF FROST ACTION

There are currently four accepted theories that have been proposed to describe the basic mechanisms of frost action of concrete aggregates (Thompson et.al. 1980). Much of the theory is based on frost action in concrete and although there is a fundamental difference between the pore-structure of concrete and that of aggregates, the basic concepts are similar.

The Powers' Hydraulic Pressure Theory (1945) proposed that hydraulic pressures caused by an advancing ice front in critically saturated pores could exceed the tensile strength of the aggregate.

Powers and Helmuth proposed Diffusion and Growth of Capillary Ice (1953) as responsible for freeze-thaw deterioration. This theory suggested diffusion of water and subsequent growth of ice crystals in capillaries as a disruptive force even at constant temperature. Differences in free energy between various phases of water and/or osmotic potentials caused by differences in solute concentration can cause diffusion. Frost deterioration has been attributed to this diffusion process.

Larson and Cady (1969) proposed a Duel-Mechanism Theory which attributes initial dilation during freezing to hydraulic pressure as proposed by Powers. Post freezing dilations measured using differential thermal analysis (DTA) suggested adsorption of water to ice and rock surfaces as a destructive mechanism. This adsorption has been referred to as an ordering process (Dunn and Hudec 1972) which is an expansive phase similar to that of water to ice.

The Desorption Theory postulated by Litvan (1972) suggested that differences in vapour pressure force the evacuation of water into and out of an aggregate. If resistance to this mass transfer of water is greater than the tensile

strength of the aggregate, rupture occurs just as in Powers' theory based on the volumetric expansion of the water-ice transformation. A more detailed description and explanation of these four accepted theories has been presented elsewhere (Thompson et.al. 1980).

It is not clear which theory or combination of theories actually represents the mass movement of water that occurs in the freeze-thaw deterioration of carbonate aggregates. Any theory which attempts to explain freeze-thaw damage should be able to explain the damage under cyclic freezing and thawing. Thus a simple volumetric expansion theory will not fully explain the process. Any theory which ignores the phase-chemistry and phase-equilibrium of liquid-solid-gas phases and effect of vapour pressure gradients in the pore-structure can not satisfactorily explain freeze-thaw effects. Coupled with such vapour pressure gradients will be an energy transfer (or potential equilization) and consequent mass transfer. Unless a distinct understanding of this phenomenon is obtained there will remain many loose ends associated with the theory which will be difficult to tie together.

It has long been recognized that the frost susceptibility of porous bodies is related to some feature of their internal structure. Litvan's Desorption Theory demonstrates the inability of water contained in micropores to crystallize in-situ and that continuous redistribution of the absorbate

on cooling to below 0 C takes place. Frost damage occurs when the process can not proceed because the amount of capillary water that is becoming unstable is greater than the flux. This process was demonstrated experimentally using porous silica glass, hydrated cement paste ,bricks and biological material (Litvan 1978).

Some of the important characteristic features of frost action in porous bodies, relative to deterioration cracking, were revealed in a desorption mechanism study (Litvan 1981). These studies indicated the following:

1.The severity of the mechanical damage caused by frost action was directly proportional to the water content of the porous solid.

2.Frost resistance of aggregates decreased with increasing size.

3.Mechanical damage was greatly increased by increased cooling rates.

4.Solids with very high or low porosities had good service records.

5.Air entrainment was an excellent method to increase the frost resistance of cement and concrete.

6.The main features of frost action appeared to be common to various porous solids.

7.Repeated freeze-thaw cycles resulted in the dessication of the porous medium and the accumulation of previously pore held liquid outside the porous solid.

8.Mechanical damage was more severe if the porous solid contained solution instead of pure liquid.

## 2.4 PORE-STRUCTURE DETERMINATION

### 2.4.1 Geotechnical Test Methods

Many laboratory techniques have been developed in an attempt to determine aggregate durability against freeze-thaw deterioration. These tests have generally been separated into two major catagories; tests based on environmental simulation and tests based on individual aggregate properties correlated to field performance. Comprehensive literature reviews of existing test procedures for frost durability evaluation for concrete have been compiled (Larson and Cady 1964) and (Thompson et.al. 1980).

#### 2.4.1.1 Environmental Simulation

This first category of tests attempts to simulate field conditions and to correlate the observed behavior to a degree of frost susceptibility. Environmental simulation tests are very useful in the development of a relative frost susceptibility criteria where no field records are available.

These criteria have been used to correlate measured pore-structure related properties such as porosity, permeability or pore-size distribution to freeze-thaw deterioration. The literature indicates that the ASTM C666 Method B Modified (Traylor 1982) is a reliable environmental simulation test. This is the method used by the University of Manitoba in the present D-cracking research program. Since environmental simulation tests do not reveal any quantitative pore-structure configuration properties they are not discussed further.

#### 2.4.1.2 Aggregate Properties

The pore-structure plays a decisive role affecting the main physical and mechanical properties of a porous body through its total volume, arrangement and distribution (topology) and the shape of the pores (morphology) (Valenta 1973). Many different tests have been developed in an attempt to correlate a specific property or specific group of aggregate pore properties to freeze-thaw durability. The pore-structure related properties that have been most commonly evaluated are ; porosity , surface area , permeability, capillarity, pore-size distribution and petrographic description.

#### 2.4.1.3 Porosity

The absorption of a porous material can be defined as capacity to receive, or absorb in it's pores, capillary free water. Absorption is a measure of effective porosity (interconnected void space/bulk volume) that expresses the volume of pores filled on attainment of equilibrium between the water pressure; hydrostatic and capillarity elevation; and the resistance; hydraulic and compressed air (Valenta 1973). This illustrates that the absorption measured in standard tests does not necessarily evaluate the total interconnected porosity volume as commonly assumed. Complete saturation is rarely obtained under normal test conditions due to trapped air and shielded porosity. This measure of porosity is directly related to the effective porosity, permeability, capillarity and the experimental boundary conditions. Separation of these variables has been found to be very difficult.

Two standard tests of absorption commonly used are the ASTM C127 and C128 which measure the specific gravity of coarse and fine aggregates respectively.

Studies of the mechanism involved in the use of high pressure water saturation were conducted using the Iowa Index Test and modified IPIT (Thompson et.al. 1980). Relationships between degree of saturation and chamber pressure were found to provide a good general index of the freeze-thaw durability. These methods did not produce conclusive

identification of an aggregate's pore-structure properties directly related to freeze-thaw durability.

Microscopic examination of polished or thin sections, stereographic procedures of point counting, linear traverse and aerial measurement are a few of the optical techniques commonly used to determine total porosity. The ASTM (C457) test includes the microscopic determination of the total porosity of the macropores but the micropore-structure remains undetected.

Pycnometer methods have been used to determine the effective porosity (Dolch 1978). The effective porosity was measured using a gas such as helium or air, a pressure vessel, Boyle's law and an independent measure of bulk density.

An absorption-adsorption technique was developed by the Portland Cement Association (Stark 1976) to determine aggregate durability. An empirical correlation was formed relating percent adsorption to percent vacuum absorption (Figure 4). Mercury porosimetry methods of porosity determination are discussed in latter sections.

#### 2.4.1.4 Pore-structure

The pore size, pore-size distribution and pore shape are a function of the pore-structure. An average or equivalent pore-size can be approximated by measuring specific surface area, permeability, absorbtivity or capillarity.

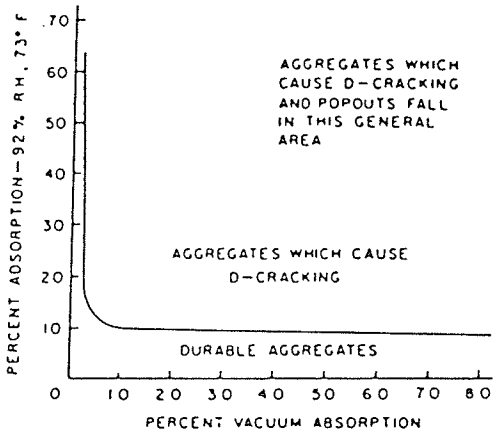


Figure 4: Absorption-adsorption curve for coarse carbonate and silicate aggregate (Stark 1976)

The adsorption of a porous body is described as the one to three molecular layers of water that are physically bonded to the solid surface area surrounding the effective porosity. Adsorption-desorption isotherms of different absorbates have been used in the determination of the distribution of surface area and pore volume (Brunauer et.al 1973, Sing 1973). Two methods of vapour phase adsorption using BET (Brunauer, Emmett and Teller) methods of micro-porosity determination have been presented (Brunauer et. al. 1973). The 'modeless' method analyzed 'wide' pores in which capillary condensation and multilayer adsorption occurred simultaneously. The second method called the 'micropore analysis method' determined parameters of the microstructure.

Because the adsorption and desorption isotherms do not coincide a hysterisis loop is formed in that particular range (Figure 5). This hysteris is a direct result of the amount of water adsorbed onto the surface of the absorbant which depends on the vapour pressure above that surface and whether the vapour is being adsorbed or desorbed. Hysterisis is a function of the pore-structure and boundry conditions of the particular test (Dolch 1978). Frost susceptibility of porous materials has been correlated to surface area measurments (Litvan 1973, 1981).

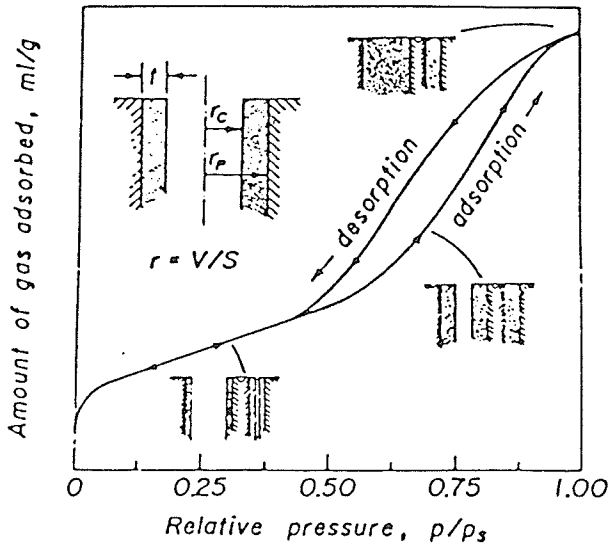


Figure 5: Absorption isotherm showing capillary condensation (Brunaeur et. al. 1973)

The permeability of a porous media is the capacity for allowing continuous flow of a liquid or gas to take place through a system of continuous pores. Permeability must be differentiated from diffusion. Porous solids allowing a flow of liquids or gas through their framework under pressure gradient show permeability. The displacement of ions or gas molecules through a porous solid under the influence of a concentration gradient is called diffusion (Zagar 1973).

Various permeating media such as water, nitrogen and air have been used to correlate permeability to D-cracking incidence (Larson et.al 1964). These procedures assume Darcy's Law is valid.

(1) $$K = \frac{QL\mu}{A\Delta P}$$

Where K = permeability coefficient, Q = volume flow rate, L = length of flow path, $\mu$ = viscosity, A = area and P = pressure differential.

The pore-structure dependant permeability coefficient is affected by the mode of mass transfer, either diffusion or capillarity. Permeability is also dependant on the effective porosity, saturation and capillarity. Correlations of permeability to freeze-thaw deterioration have not been conclusive.

Diffusion measurements have been used for the pore-structure determination of porous media (Hesse 1973). The measured values obtained were related to the pore-structure but any quantitative evaluation was uncertain.

Capillarity action is the suction force exerted on a wetting fluid such as water ($0<90^{\circ}$) that is inversley proportional to the radius of the pore. An idealized model of capillary suction of a capillary tube of radius r is given in Figure 6. Using the law of Hagen-Poiseville the following relationship was developed:

(2) $$P = \frac{2\gamma\cos\theta}{gr}$$

Where P = suction force, $\gamma$ = surface tension, $\theta$ = contact angle of fluid, g = acceleration due to gravity and r = pore radius.

Aggregate and mortar capillarity have been measured and correlated to frost susceptibility (Larson 1964). The idealized pore-structure model of bundles of different size capillary tubes differs substantially from the actual pore-structure. Therefore no quantitative aggregate or pore structure measurements can be accurately obtained from these tests. Investigations of capillary rise of electrolytic solutions have been investigated (Gribanova et.al 1973). Evaporation techniques of pore diameter and permeability deter-

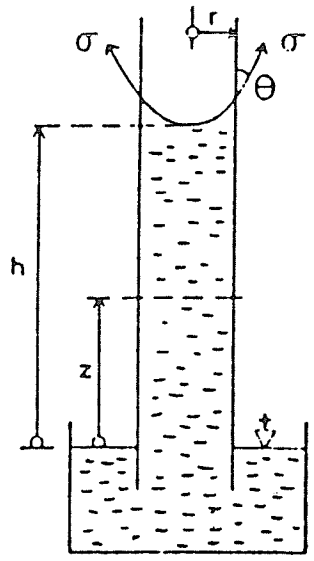


Figure 6: Capillary suction

mination used for freeze-thaw deterioration correlations have resulted in inconclusive parameters (Brown 1968).

### 2.4.1.5 Pore-size Distribution

Mercury intrusion porosimetry has been found to be the the most common method for pore-structure determination in recent geotechnical aggregate studies. In principle it is the reverse action of capillary suction. The surface tension of a non-wetting fluid ($0>90^{\circ}$) prevents it from entering a pore space. This phenomenon is called capillary depression. By applying an external pressure to the liquid the capillary force is overcome and the liquid enters the pore. This pressure is a function of the surface properties of the liquid and solid involved and the pore-structure.

(3)
$$P = - \frac{4\gamma\cos\theta}{d}$$

Where P = pressure, d = pore diameter, $\gamma$ = surface tension and $\theta$ = contact angle. The bundle of capillary tubes of varying size model has been assumed for the calculation of the pore-size distribution.

Mercury porosimetry has been used to correlate frost durability with the pore-size distribution of the coarse carbonate aggregate fraction of the concrete (Dolch 1978, Kaneuji et. al. 1980). Test results for various aggregates relating cummulative pore volume to limiting pore diameter are illustrated in Figure 7. An empirical durability criteria was developed relating a pore-structure derived expected durability factor (EDF) to observed field performance (Kaneuji et. al. 1980). Correlations between the predicted EDF values and freeze-thaw durability determined by ASTM C666 B Modified have been reported (Kaneuji et. al. 1980, Lindgren 1980).

Low-pressure and conventional-pressure MIP have two major drawbacks. First, the pore diameters recorded are not necessarily the true pore diameters, as assumed by the capillary tube bundle model, but are the pore entry diameters of the pore network. Second, there exists 'lost porosity', which is attributed to the inability for the mercury to in-

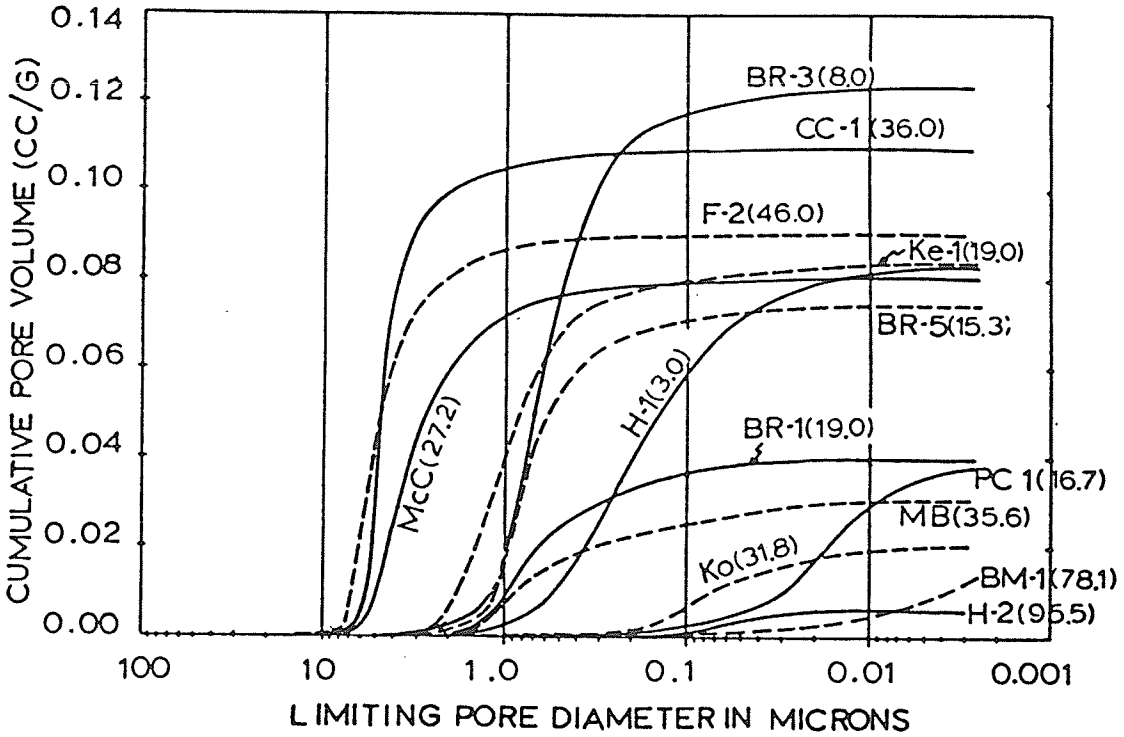


Figure 7: Pore size distributions of test aggregates (Kaneuji et. al. 1980)

vade the complete pore network of the aggregate (Alford et.al. 1981). The pore-size distribution calculations are therefore weighted towards the fine end of the pore-size range by the presence of these 'ink bottle' pores which shield larger connected pores from lower pressure intrusion.

An evaluation of hysterisis in mercury intrusion porosimetry by depressurization and second intrusion reported on the effect of 'ink bottle' pores (Cebeci et. al. 1978). Secondary intrusion was found to be helpful in distinguishing pores of uniform cross-section from ink bottle pores. Calculations of the distribution of uniform pores and the volume

of 'ink bottle' pores intruded at each entrance diameter were obtained.

The addition of analysis during depressurization and second intrusion resulted in more comprehensive pore-structure information than could be obtained by conventional MIP tests. To date there is no record of this method being used in the investigation of the freeze-thaw deterioration of carbonate aggregates.

Calorimetric determinations of pore-size distribution have indicated a relationship between the pore-size , the triple-point temperature of water and the heat of solidification (Eyraud et.al 1973). This procedure of analysis assumed the measurement of pore radius rather than pore opening. Litvan (1973) points out that capillary water does not freeze in-situ which was an inherent assumption used in this pore structure analysis.

Adsorption-desorption isotherm methods for pore volume description have been presented and discussed earlier (Brunauer et.al 1973).

#### 2.4.1.6 Petrographic Description

Petrographic examination of concrete aggregates is the science of the description and classification of rocks. Detailed description of the various pore related parameters such as minerology, surface texture, porosity, permeability

and fabric are described. Identification of an aggregate's constituents aids the recognition of various porosity types and the associated pore-structures which ultimately influence the freeze-thaw durability.

Common techniques frequently used in geotechnical petrographic analysis have included the use of thin sections, hand lens, petrographic and stereographic microscopes, scratch tests, HCl treatment and carbonate staining. Less commonly reported tests are X-ray diffraction and scanning electron microscopy (SEM). Regular petrographic description techniques have been found inadequate in distinguishing micro porosity types (<15 microns) important to freeze-thaw durability. Further analysis of many freeze-thaw durability related studies has often been inhibited due to limited petrographic description of the aggregate involved. Comprehensive petrographic description has been found necessary for a complete freeze-thaw deterioration analysis (Hiltrop et.al. 1959, Larson et.al. 1965, Shakour et.al. 1982).

SEM and X-ray diffraction have been successfully used for the qualitative determination of minerological composition of carbonate aggregates (Mysyk et. al. 1985). A modified petrographical examination procedure including SEM and X-ray diffraction is essential for a complete pore-structure analysis of carbonate aggregates.

A general lack of understanding of the basic mechanisms involved in the phenomenon of freeze-thaw deterioration has lead to the development of many inventive test procedures in an attempt to identify nondurable aggregates. The bulk of the standard tests presently used are empircally inaccurate and misleading. Various methods of porosity evaluation and the parameters measured are listed in Table 4. The data obtained has been correlated directly to imposed boundary conditions and test environments using simplified model assumptions that often bear little relevance to the actual pore structure analyzed.

Pore analysis is difficult due to the fact that characteristics and properties of pore systems such as absorption, porosity, permeability and capillarity are closely interrelated and it is difficult if not impossible to evaluate the effects of each separately.

In very few studies has there been any attempt to accurately describe the actual pore structure under investigation before adopting a simplified pore model. Pore models have generally been chosen to facilitate simple analysis rather than to describe the actual pore system. Limited petrographic sample description renders the data obtained in such studies useless for further investigation.

Before a study can even attempt to investigate a phenomenon such a D-cracking, a comprehensive look at the physical

make-up of the materials involved must be undertaken. Concise and accurate sample description is a fundamental component of any aggregate investigation.

TABLE 4

Methods of porosity measurement (Racic 1984)

| | | | Total porosity | Saccate porosity | Open porosity | Permeable poros. | Micropore volume | Specific surface | Mean pore size | Pore size distn. | Pore shape |
|---|---|---|---|---|---|---|---|---|---|---|---|
| DIRECT | STEREOLOGY | Phase integration; areal analysis | × | | | | | | | | |
| | | Lineal analysis; point-counting | × | | | | | | | | |
| | | Intercept analysis | | | | | | × | × | × | × |
| | | Serial sectioning | | | | | | | | × | × |
| INDIRECT | FLUID DISPLACEMENT | Buoyancy | × | | × | | | | | | |
| | | Pycnometry | × | | × | | | | | | |
| | | Gas volumetry | | | × | | | | | | |
| | FLUID FLOW | Transient gas flow | | × | × | | | | | | |
| | | Steady gas or liquid flow | | | | × | | × | (a) | | |
| | INTERFACIAL CURVATURE | Suction & pressure porosimetry | | | | | | (b) | | × | |
| | | Capillary condensation | | | × | | | (b) | | × | |
| | | Freezing-point depression | | | | | | (b) | | × | |
| | ADSORPTION | Adsorption of gases & vapours | | | | | × | × | (c) | | |
| | | Adsorption from solution | | | | | | × | (c) | | |
| | | Molecular sieve effects | | | | | (d) | | | | |
| | | Heat of wetting | | | | | | × | | | |
| | OTHER | Electrical conductance | | | | × | | | | (e) | |
| | | Radiation attenuation | × | | | | | | | | |
| | | Rediation scattering | | | | | | × | × | | |
| | | Wetting kinetics | | | × | | | | × | | |

(a) Size of equal cylindrical pores of same total volume, giving same permeability.
(b) Calculated by integration — see, p. 000.
(c) Calculated from surface-to-volume ratio, if porosity is also known.
(d) Can give size-distribution of micropores.
(e) By Astbury's method, based on wetting kinetics.

### 2.4.2 Geological Test Methods

Geological test methods of pore-structure evaluation differ substatially from the geotechnical test methods described. Most techniques deal with the geology of carbonate porosity and the classification of reservoir rocks for petroleum recovery potential. Pore-structure examination details both macroscopic and microscopic mineral grain and pore structure analysis. Various geological methods of pore-structure evaluation are reviewed and the important aspects are discussed.

#### 2.4.2.1 Teodorovich's Method

Teodorovich's method, based on petrographic analysis, suggested a quantitative relationship between permeability and the pore-structure characteristics (Aschenbrenner et.al. 1960). An empirical equation of permeability was formed using various pore characteristics such as the character of pore and pore necks, width and number, effective porosity, average size, shape and type of pore. The empirically derived permeabilities were correlated to measured permeabilities. This technique, originally developed for optical microscopy, could be applied to microporosity determination using SEM or optical techniques.

### 2.4.2.2 Classification of Rocks by Surface Texture

This method correlated visual rock characteristics to measured reservoir properties of carbonate rocks and sandstones (Robinson 1966). Polished sections or thin sections were viewed under binocular microscopes and classified according to surface texture. The measured reservoir properties were porosity, permeability and pore-size distribution.

The surface textures described were; smoothness, granular open- texture, granular closed-texture, granular clogged-texture, visible pore spaces and vugs. The four types of carbonate rocks used were, partly dolimitized limestone, dolomite, fine matrix limestone and dense carbonate.

The effective porosity was determined using bulk volume determination by mercury displacement , grain volume determination using Boyle's law and gas expansion applications. Air permeability was measured using pressures ranging from one to two atmospheres. Pore-size distribution was measured by mercury injection and capillary pressure curves.

The empirical correlation formed between rock texture and measured pore properties enabled the prediction of reservoir properties using petrographic description. This technique could be useful for the evaluation of freeze-thaw susceptibility of carbonate aggregates using micro and macro-porosity surface texture classification.

#### 2.4.2.3 Mathematical Modelling

A mathematical procedure for calculating the porosity and permeability of a porous body was developed using a random pore-size distribution (Talash et. al. 1965). This technique adapted Poisseville's equation and Darcy's law to a random number generator on a digital computer. This procedure allowed for a quantitative computer analysis of a wide variety of random pore configurations and distributions and their effects on permeability and porosity.

#### 2.4.2.4 Mercury Intrusion-Extrusion Porosimetry

The use of pore casts and capillary pressure for the determination of pore geometry has greatly improved the usefulness and understanding of mercury porosimetry (Wardlaw 1976). This study was aimed at more accurately describing complex carbonate pore-structures in terms of the pores and pore connections (pore throats) and investigating mercury porosimetry by the use of mercury-injection ejection procedures.

SEM photos of pore casts of dolomitic limestone revealed that the pore throats could be more accurately described as sheet-like rather than tubular. This indicated that the pore system was inaccurately represented by the bundle of capillary tubes model. A more appropriate interpretation was presented.

(4) $$P_c = - \frac{2\sigma\cos\theta}{d}$$

Where $P_c$ = capillary pressure, $\sigma$ = surface tension, $\theta$=contact angle and d = distance separating parallel plates.

The volume of mercury entering an evacuated pore system during successive pressure increments was plotted as a pressure volume curve, referred to as a capillary pressure curve. Mercury ejection curves were obtained on pressure reduction. Capillary pressure curves indicated that samples having very similar mercury intrusion curves showed markedly different behavior during pressure reduction (Figure 8). Second intrusion indicated pore-structure characteristics undetected by mercury intrusion. The pore characteristic believed to be responsible for this phenomenon has been attributed to the presence of 'ink bottle' pore-structure. Mercury-injection ejection and reinjection have been used to determine additional information of the pore-structure (Figure 9).

The volume of mercury entering a sample between specific pressure limits is related to the fraction of the total pore volume that is connected by pore throats that are within the specific pressure-size limits. During injection the large interior pores and pore throats may be shielded from mercury intrusion if they are connected by smaller throats. This re-

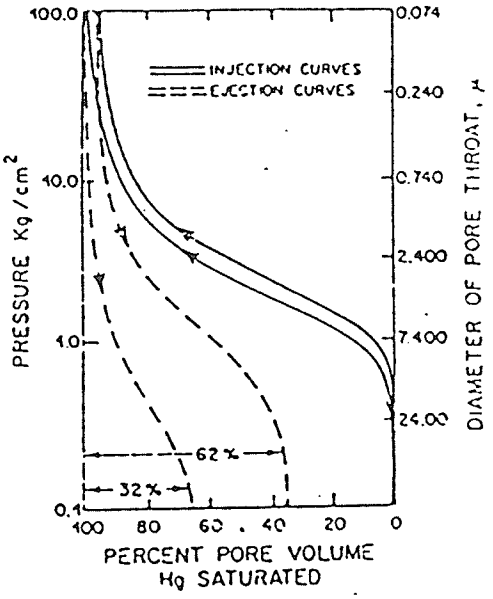


Figure 8: Mercury-injection and ejection capillary curves for two Rainbow Lake dolomite samples (Wardlaw 1976)

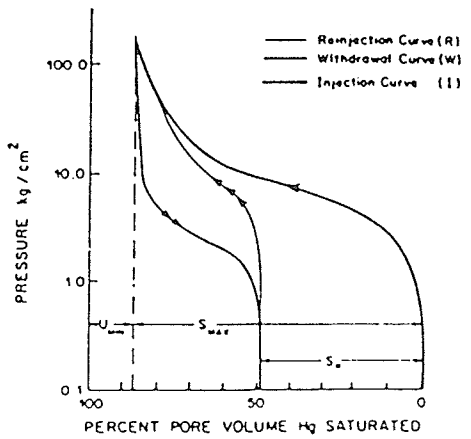


Figure 9: Capillary pressure diagram illustrating terms defined in the text (Wardlaw and Taylor 1976)

sults in an 'apparent' volume accessible through throats within that specific size range. Investigations of mercury-injection ejection hysterisis and artificial and theoretical pore-network models indicated that some of the significant aspects that affect behavior of the pore-structure are; pore diameter to pore throat diameter, throat to pore coordination number or connectivity and extent of random and non-random homogenities within the system (Wardlaw 1981).

#### 2.4.2.5 X-ray Diffraction

Mineralogical identification of carbonate rock constituents has been determined using X-ray diffraction. Calcite-dolomite ratios have been obtained using peak height analysis of X-ray diffractographs (Mysyk 1985). Sample preparation is very simple, an X-ray scan can be completed in minutes and the results give an accurate indication of the relative mineral composition of the sample analyzed. X-ray techniques are useful for confirming minerological identification by SEM photography. The pore-structure and strength of carbonate aggregates are a direct function of the minerological composition. X-ray diffraction provides good estimate of the percent composition of the mineralogy of aggregates under petrographic examination.

### 2.4.2.6 Pore Casting

Pore casting (epoxy resin replicas of pore space) is a well known means of pore-structure examination of carbonate rocks (Pittman et.al. 1971, Wardlaw 1976). This procedure combines vacuum evacuation with subsequent pressure application in a pressure vessel that impregnates a low viscosity resin into the interconnected microstructure of a test aggregate. The impregnated resin compound used for these pore casts have been dyed for optical recognition. If a colored dye is not feasable, flourescent dyes can be used for subsequent microscopy in ultra violet illumination. After grinding and polishing (> 1 micron) the specimens can be etched with dilute HCl and HF acid to remove the carbonate host leaving a relief profile of the pore-structure. Pore-structures of down to 0.1 micron have been impregnated (Wardlaw 1976).

Both the macro and microstructures of impregnated samples can be analyzed through the use of optical microscopy or SEM procedures. SEM photographs of mineral grain structure and corresponding pore casts have been used to analyze carbonate microstructure (Figure 10).

Methods of 3-D pore geometry analysis have been attempted using 'double pore cast' impregnation (Lin et.al. 1983). Samples were continuously polished and photographed in 5-10 micrometer slices effectively analysing the 3-D pore-struc-

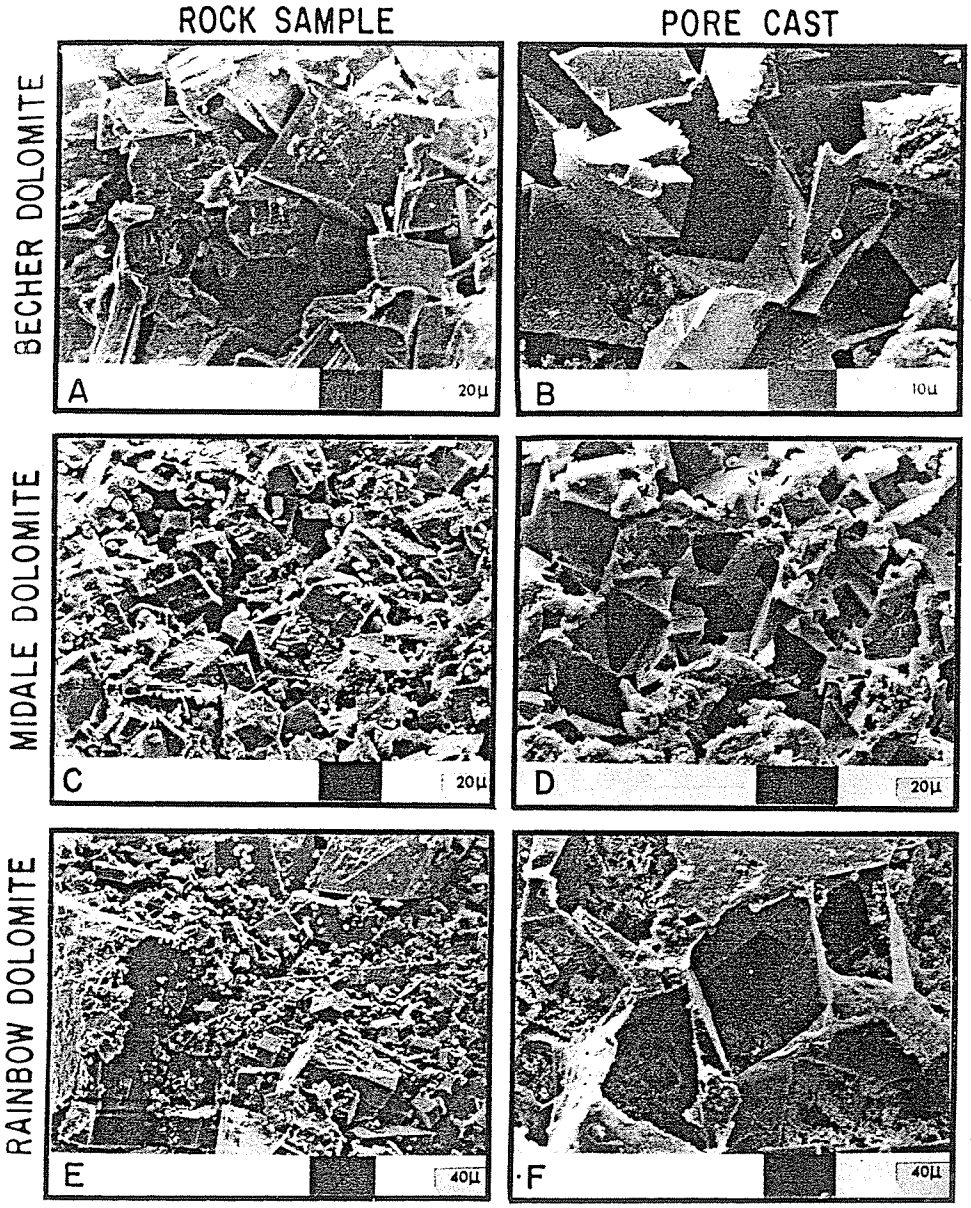


Figure 10: Scanning electron micrographs of three rock samples and corresponding pore casts (Wardlaw and Taylor 1976)

ture. This procedure was carried out using optical microscopy and SEM procedures. The analysis procedure input serial-section images into an image analysis computer which produced a 3-D image using computer graphics. One disadvantage of this procedure was that the delicate sample preparation techniques were very time consuming. The procedure provides a valuble extension to conventional SEM pore cast and image analysis techniques.

Pore casting provides a means for the direct investigation of the 2-dimensional pore structure of the effective porosity intrudable by a low viscosity epoxy resin. Some of the parameters that have been measured are the effective porosity, surface area, pore shape and size, pore throat shape and size, pore distribution, pore to throat ratios and connectivity (Wardlaw 1976). Efficient processing of this pore-structure information is done most effectively using image analysis computer procedures.

There are various problems that can arise during sample preparation of pore casts. If the material contains hard brittle particles these may be torn out and possibly reimbedded in a different part of the surface during polishing. If too much pressure is applied during polishing the surface may become badly distorted. Great care must be taken so that the pore cast is not smeared over adjacent mineral grains. If the specimen contains constituents that differ appreciably in hardness the removal of the softer grains produces a

relief profile. Other limitations of pore casting are that isolated porosity may not be intruded and high pressure of resin intrusion may produce pore cast collapse. There also remains the question of the statistical significance of the 'representative sample' under investigation.

### 2.4.2.7 Scanning Electron Microscope (SEM)

The scanning electron microscope (SEM) uses an electron beam approximately 100 A° in diameter to scan a sample. The secondary radiation produced from this scan is detected and transformed to a visual image on a cathode ray tube (CRT). In this form the body under investigation can be photographed or sent to a computer monitor and digitized. The magnification can be varied from about 20X to a maximum of 40,000X. The SEM has the advantage of possessing a very large depth of field often 100X greater than that of an optical microscope at the same magnification.

The SEM has been used extensively to provide qualitative information of the pore geometry of carbonate rocks, either directly (Timur et.al 1971, Pittman et.al 1979) or indirectly by the examination of pore casts (Pittman et.al. 1970, Wardlaw 1976, Wardlaw et.al. 1976). SEM photographs of epoxy pore casts have been used for the qualitative analysis of 2-dimensional images of sedimentary rock pore-structure.

Although the images produced reveal very useful qualitative information about carbonate porosity they do not serve easy quantitative analysis procedures due to the nature of the image. Very delicate and intensive techniques are required to facilitate quantitative description of SEM photographs using image analysis. Also such samples often possess very little statistical significance in relation to the bulk sample.

## 2.5 IMAGE ANALYSIS

In the simplest terms image analysis is a facet of stereology that quantitatively evaluates the statistical and geometrical properties of 2-dimensional images. Image acquisition techniques that have been used for pore-structure analysis are optical and SEM microscopy, photographs, negatives, reflected light from planar sections or transmitted light through thin sections. Image Analysis Procedures (IAP) (Rink 1973, Rink and Schopper 1976, 1978) and Petrographic Image Analysis (PIA) (Ehrlich et.al. 1984, 1985) techniques have been well developed and extensively used in pore-complex research.

This section describes some of the stereometric parameters, features and characteristic shapes commonly used in image analysis. Basic Petrographic Image Analysis (PIA) techniques for the analysis of reservoir pore-complexes are discussed. This discussion includes erosion-dilation algor-

ithms of pore analysis as well as some advanced data acquisition, processing and presentation models. Several other very basic pore-structure analysis models and procedures are introduced and comparisons between standard tests evaluated.

Detectable images are obtained using a video-camera system integrated with an analog/digital converter that electronically digitizes these images into a matrix of binary data. Each picture point in the image matrix, referred to as a 'pixel', is defined by three values: two spatial coordinates (X,Y) and a 'grey level' intensity value (Ehrlich et.al. 1984). A micro or macro-computer is used to process these digital images using various complex pattern recognition algorithms and data manipulation computer programs. Basically image analysis is accomplished by: a) scanning and sampling the planar image b) selection and recognition of features and c) counting, analysing and processing the data into a usable form.

The description of the pore-structure involves the determination of five independent stereometric parameters; size, shape, particle or pore density, distribution and orientation. Features and characteristic shapes commonly used in image analysis have been identified by certain form functions. Some useful form factor quotients that have been defined are illustrated in Figure 11. Image analysis procedures have been used to separate these individual section figures on the basis on grey-level recogntion, count them

and calculate a host of size and shape parameters and statistical distributions (Figure 12). These parameters have been used to express the influence of the microstructure on the physical and chemical properties of a body (Nazare et. al. 1973). Both organic and inorganic substances have been evaluated (Fischmeister 1973).

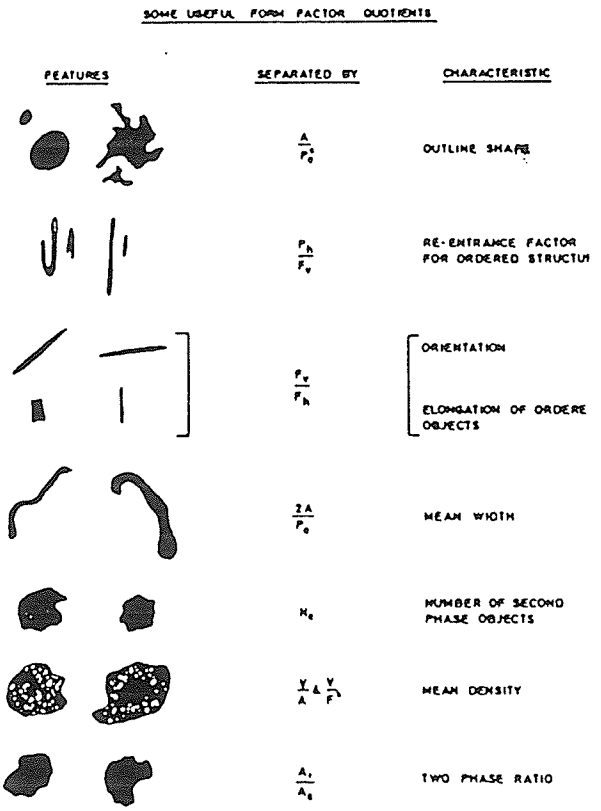


Figure 11: Some useful form factor quotients (Terrell 1973)

Theoretical analysis presented demonstrates that a)the volumetric porosity (void volume/total volume) of a specimen can be expected to equal the aerial porosity (void area/to-

*Morphometric parameters determined by automatic image analysis*

| Symbol | Meaning |
|---|---|
| $a$ | area |
| $d_\omega = 2\sqrt{\frac{a}{\pi}}$ | diameter after WADELL |
| $c$ | circumference |
| $m = a/c$ | hydraulic radius |
| $k_h = c/2\sqrt{\pi a}$ | shape factor after HEYWOOD |
| $k' = 4\pi a/c^2$ | shape factor |
| $h$ | height } tangent diameter { ↕ |
| $w$ | width } after FERET { ↔ |
| $p$ | } total projection { ↕ |
| $q$ | } total projection { ↔ |
| $k_{c\bar{v}} = \frac{p+q}{h+w}$ | concavity factor |
| $s_{max.l}$ | max. intercept length (KRUMBEIN) ↔ |
| $s_{ml} = a/p$ | } mean intercept length { ↔ |
| $s_{mc} = a/q$ | } mean intercept length { ↕ |
| $l$ | approx. longest extension |
| $d_m = a/l$ | mean intercept length $\perp l$ |
| $k_e = l/d_m$ | elongation factor |
| $\left.\begin{matrix} e_1 \\ e_2 \end{matrix}\right\} = \frac{2}{3\pi}\left[c + \sqrt{\pi a} \pm \sqrt{(c+\sqrt{\pi a})^2 - 9\pi a}\right]$ | axes of equiv. ellipse (MOORE) |
| $\left.\begin{matrix} r_1 \\ r_2 \end{matrix}\right\} = \frac{1}{4}(c \pm \sqrt{c^2 - 16a})$ | sides of equiv. rectangle (MOORE) |

↔ line direction ↕ column direction

Figure 12: Morphometric parameters determined by automatic image analysis (Rink and Schopper 1976)

tal area) b) the volumetric specific surface (void surface/ total volume) can be expected to equal the aerial specific surface (void perimeter/total area) measured on a 'representative' cross-section (Martin 1973). This is true assuming the spatial pore distribution in the rock is statistically homogeneous and isotropic. This is rarly true in most natural porous bodies. This makes extrapolation from 2-dimensional images to 3-dimensional pore-structure difficult. There must be some relationship (termed transfer func-

tion) between the pore-complex intersected by a plane and the 3-dimensional network (Ehrlich et. al. 1984).

The physical properties of sedimentary rocks strongly depend on the geometric structure of their pore space. Geometric analysis of the pore-structure has been used to provide valuable quantitative information on formation evaluation (Rink et. al. 1978). Polished sections of four epoxy resin-impregnated sandstone samples were evaluated. Some of the parameters measured were porosity, surface area, capillarity, hydraulic radius and hydraulic permeability. Mathematical derivations of these parameters obtainable by image analysis were described. Comparisons of pore-structure data obtained by these techniques were made with various physical measurements.

The porosity obtained stereologically by image analysis compared favourably to volumetric determinaton. The quality of the image data depended on the quality of the impregnated pore space, the optical contrast and boundary delineation. These can be improved by proper sample polishing techniques and the proper setting of the light, focus and grey level threshold on the computer.

The differently derived values of specific surface were in poor agreement. Gas adsorption methods produced extremely large values. Similarly large values obtained for capillarity were suspect of integration errors at the high pressure

end of the curve. The extremely low values found by image analysis may have been due to the limited resolution of the scanning system for very small pores.

Good agreement was found between the mean hydraulic radius derived physically from capillarity curves and by image analysis. Permeability showed varying degrees of agreement between physical data and image analysis. This can be expected due to the uncertain nature of the physical test and the model assumption used for these analysis procedures.

Petrographic Image Analysis Techniques (PIA) for the analysis of reservoir pore complexes have been developed (Ehrlich et. al. 1984). These procedures, utilizing a specially designed computer, have been used to generate large arrays of different variables of a given image. Some of the variables that have been measured are listed in Table 5. These variables are however not statistically independent and can be linked to smaller subsets using linear transformations. This procedure is referred to as 'factor analysis' (orthoganalization).

One pore-analysis algorithm used in PIA studies utilizes procedures of erosion and dilation for the analysis of image features. In order to understand this erosion-dilation algorithm the basics of erosion and dilation procedures must first be explained. The concept of erosion has been described as a prarie fire burning inwards from the perimeter

TABLE 5

PIA pore complex geometry variables (Ehrlich et.al. 1984)

| | | | |
|---|---|---|---|
| MX1 | Mean number of pores | ST1–ST29 | Throat size (microns) |
| MX2 | Mean number of throats | | |
| MX3 | Mean number of pores with throats | ST1 | ≤20 |
| MX4 | Mean total pore area | ST2 | >20–40 |
| MX5 | Mean smooth pore area | ST3 | >40–60 |
| MX6 | Mean rough pore area | ST4 | >60–80 |
| MX7 | Mean area of pores with throats | ST5 | >80–100 |
| MX8 | Mean perimeter | · | |
| MX9 | Mean weighted area of flow normal to section | · | |
| | | · | |
| MX10 | Mean weighted area of flow parallel to section | ST26 | >500–520 |
| | | ST27 | >520–540 |
| MX11 | Mean bending energy | ST28 | >540–560 |
| MX12 | Ratio of mean smooth pore area to mean rough pore area | ST29 | >560–1,180 |
| MX13 | Ratio of mean pore area to mean number of pores | SC1–SC30 | Pore coordination number intervals |
| MX14 | Ratio of mean total perimeter to mean number of pores | SC1 | Number of pores with 1-fold coordination |
| MX15 | Ratio of mean bending energy to mean number of pores | SC2 | Number of pores with 2-fold coordination |
| | | SC3 | Number of pores with 3-fold coordination |
| MX16 | Ratio of smooth pore area to mean number of pores | SC4 | Number of pores with 4-fold coordination |
| | | · | Number of pores with · coordination |
| MX17 | Ratio of number of pores with throats to mean number of pores | · | Number of pores with · coordination |
| | | · | Number of pores with · coordination |
| MX18 | Ratio of total area of pores with throats to mean number of pores with throats | SC30 | Number of pores with 30-fold coordination |
| MX19 | Ratio of mean area of pores with throats to mean number of pores with throats | | |
| Top | Mean total optical porosity | | |
| Perent 1 | Proportion of pore type 1 (see text for descriptions) | | |
| Percent 2 | Proportion of pore type 2 | | |
| Percent 3 | Proportion of pore type 3 | | |
| Percent 4 | Proportion of pore type 4 | | |

| SS1–SS10 | Smooth porosity intervals (microns) | | RR1–RR9 | Rough-porosity intervals (microns) | |
|---|---|---|---|---|---|
| SS1 | ≤20 | | RR1 | ≤20 | |
| SS2 | >20–40 | | RR2 | >20–40 | |
| SS3 | >40–60 | Maximum | RR3 | >40–60 | Maximum |
| SS4 | >60–80 | entropy | RR4 | >60–80 | entropy |
| SS5 | >80–100 | spectral | RR5 | >80–100 | spectral |
| SS6 | >100–120 | intervals | RR6 | >100–120 | intervals |
| SS7 | >120–160 | | RR7 | >120–160 | |
| SS8 | >160–200 | (Full et al. 1984) | RR8 | >160–260 | (Full et al. 1984) |
| SS9 | >200–320 | | RR9 | >260–1,180 | |
| SS10 | >320–1,180 | | | | |

evenly on all sides. One erosion cycle performed on an individual pore is the removal of the outer most layer of pixels from the object or pore segment. Dilation is the reverse of erosion where a layer of pixels is added to the object. It is important to realize that dilation after an erosion does not necessarily restore the object to the original shape. As erosion-dilation cycles, proceed pores of progressively larger size are lost and the surviving elements are of simpler geometry. After x number of erosion cycles, if a seed pixel still exists, subsequent dilation will occur x times. However, if no seed pixel exists and the pore has disappeared, the size of the pore before the erosions occurred is defined as the pore porosity. The difference between this segment and the original pore segment is defined as the roughness porosity.

These procedures are illustrated in Figure 13. Image A and A' represent the original pore-structure. The effect of erosion is that it strips off the outer layers or 'pixels' of the image illustrated by image B. Dilation is the opposite of erosion in that it adds 'pixels' to the defined image. Image B undergoes dilation and produces image B'. The image is further eroded producing image C and subsequent dilation produces image C'. It is noted that the large pores have smoother surfaces and the smaller pores are absent.

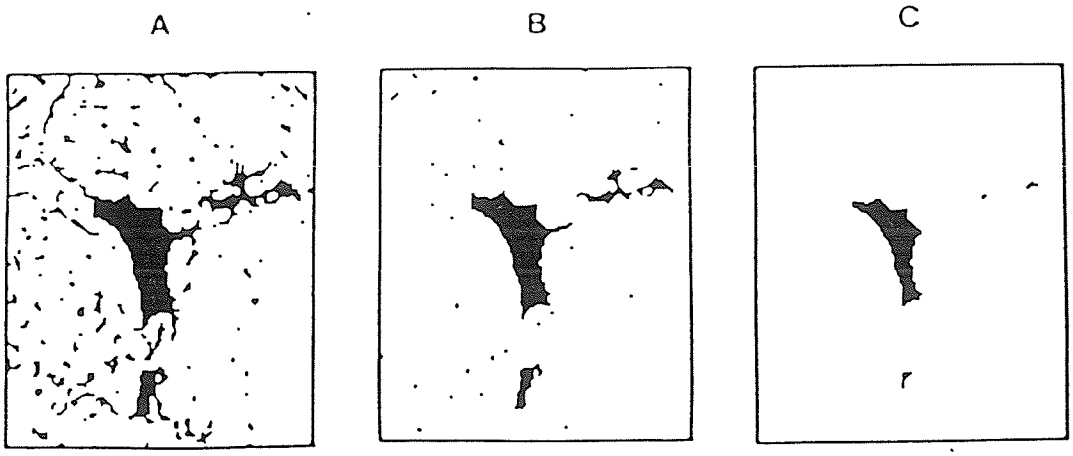


-A) A portion of the binary image in Figure 3 showing micropores, large pores, and pore roughness elements; B) same field of view after erosion of one pixel layer; and C) after erosion of three pixel layers.

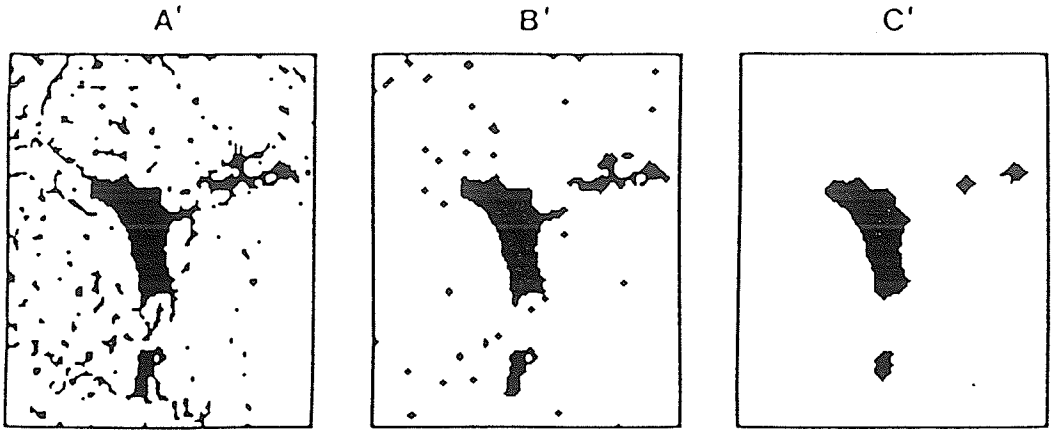


Same sequence but showing subsequent dilation after erosion. After one cycle (B'), the micropores and surface roughness of the three larger pores have been lost. After three cycles (C'), all small pores have been lost, the larger pores have smooth surfaces (especially note the loss of the "spur" on the largest pore between B' and C'), and a pore has been severed.

Figure 13: Erosion and Dilation of computer images (Ehrlich et.al. 1984)

Pattern recognition/classification algorithms have been developed that consist of monitoring the proportion of the porosity that is 'lost' under progressively more severe cycles of erosion-dilation. Each cycle began with the original image of a single pore-segment selected from the field of view under investigation. The pore-segment underwent erosion-dilation cycles until at some point the entire pore disappeared and the dilation had nothing to restore. The

portion of the pore that exists just before this occurs is referred to as the 'pore porosity'. The proportion of the rest of the porosity of that pore that is monitored with each cycle is referred to as 'roughness porosity'. Analyzing all of the pores in a given field of view in this manner results in a frequency distribution of the proportions of the total porosity lost each cycle, the total being 100%. These frequency distributions have been termed 'pore-complex spectra'. An example of 'pore complex spectra' for a given image is illustrated in Figure 14. The porosity has been divided into a bimodal-size distribution and roughness distribution.

Algorithms referred to as QMODEL's have been designed that represent a sample as a linear combination of three pore types (Figure 15). This figure can be considered to be a mixture of varying proportions of three types of pores. The pore types represent discrete stages of porosity development. EM-1 represents large extended pores of complex geometery, EM-2, small relatively smooth pores and EM-3, pores associated with fine and coarse grained sands. Each point represents a multidimesional vector(spectra), which in turn represents a sample pore type. Expansion of the complex statistical theory associated with this algorithm is beyond the scope of this discussion.

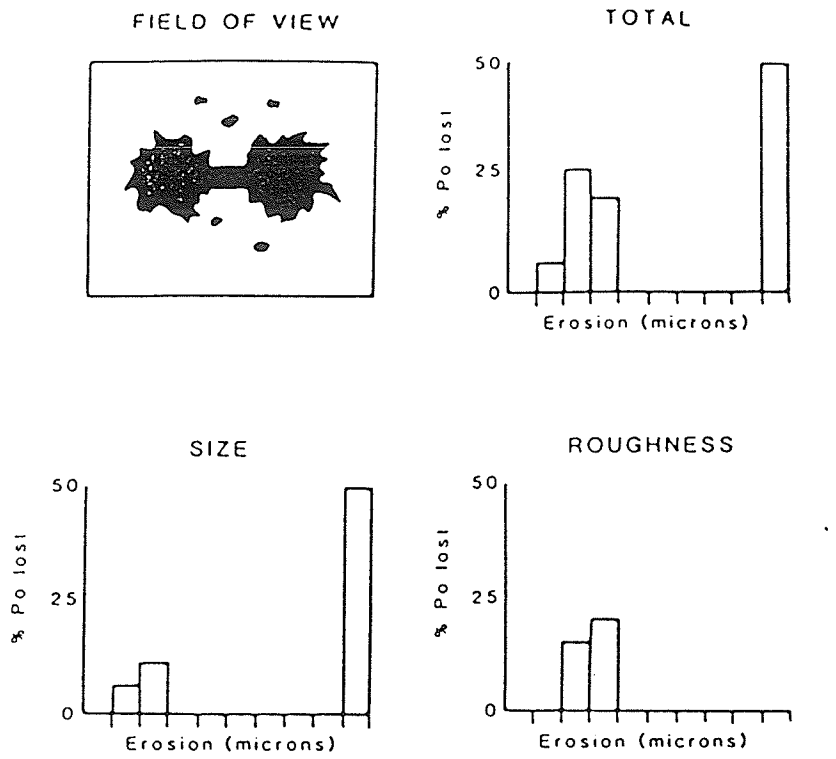


Figure 14: A complex field of view showing the total porosity loss partitioned into a bimodal-size distribution and a roughness distribution (Ehrlich et.al. 1984)

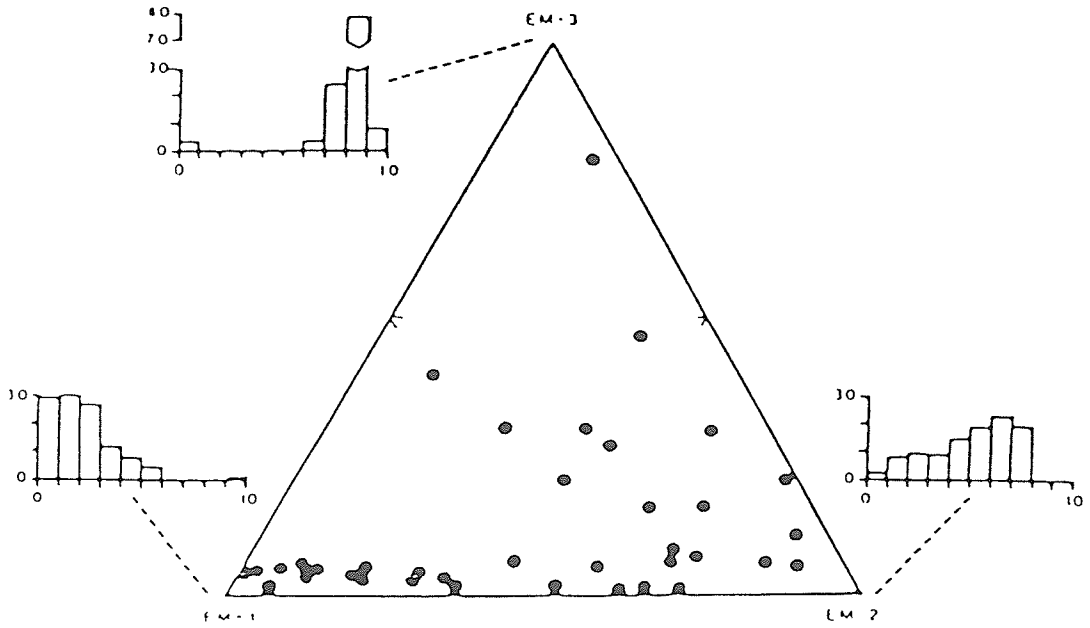

Figure 15: FUZZY QMODEL (Ehrlich et.al. 1984)

Rock types including both clastic and carbonates have been investigated. High correlations between image parameters and physical tests such as permeability and residual saturation have been obtained(Ehrlich et.al. 1984). So far small subsets of PIA variables have consistently produced equations which estimate permeability and other flow properties with high precision.

Similar studies of quantitative petrography of carbonate rocks by image analysis have been reported (Harvey et. al. 1972). Relative mineralogical and textural properties of different carbonate rocks were evaluated. Measurements were conducted on polished and etched specimens, standard thin sections and on scanning electron micrographs. The quantities measured were dolomite content, pore volume, pore boundary projection and pore-size distribution. Relative values of these parameters were used for the characterization of carbonate rock materials.

Investigations of quantitative stereology analysis of pore-size distribution in sandstone have been presented by Dullien (1973). Two pore models were adopted for the stereographic pore-structure analysis, the Sphere Segment (SPS) model and the General Pore Segment (GPS) model. The SPS model approximated the pore-structure by a 3-D network of strings of touching spheres distributed over a range of diameters. The GPS model is similar to the SPS model except that the pore segments are irregularly shaped objects. The

GPS model was found to fit experimental results more closely.

The pore-size distribution evaluated by mercury porosimetry and photomicrographic methods on identical samples differed drastically in every case (Figure 16). These are the results that can be expected due to the nature of mercury porosimetry that yields the distribution of pore volume controlled by pore neck diameter. The peak of the pore size distribution curve has been accepted as a measure of 'mean pore neck diameter' and it is also generally accepted that the actual pore-structure is more accurately defined using photomicrographic methods. The SPS model of pore-structure analysis has been used on pore casts of NACL particles. Comparisons of these photomicrographic techniques have been made with sieve analysis (Figure 17).

Comparisons between stereological determination, using both linear and aerial determinations, and mercury porosimetry on four types of porous nickel specimens showed good correlations (Ministr 1973). The limitations of both test methods must be kept in mind when comparing results. Assuming the absence of 'ink bottle' pores, the Ni specimen comparison is valid.

Image analysis methods have been presented for the evaluation of the air void structure of concrete (Racic 1984,

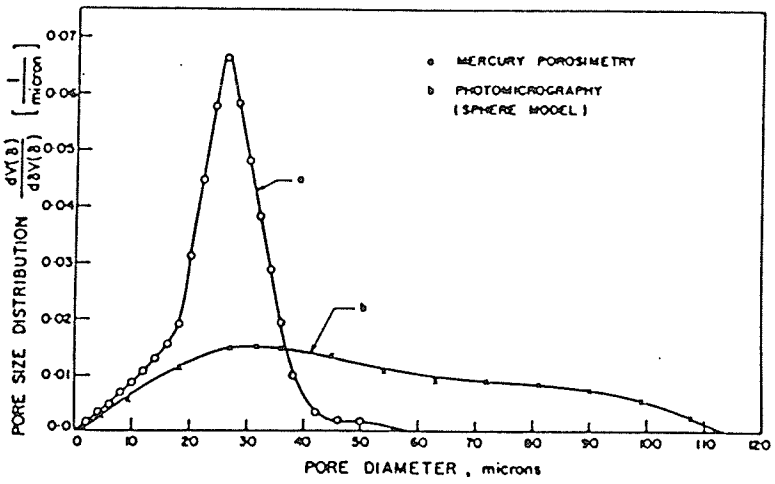


Figure 16: Comparison of mercury porosimetry and photomicrographic pore size distribution curves for torpedo sandstone (Dullien 1973)

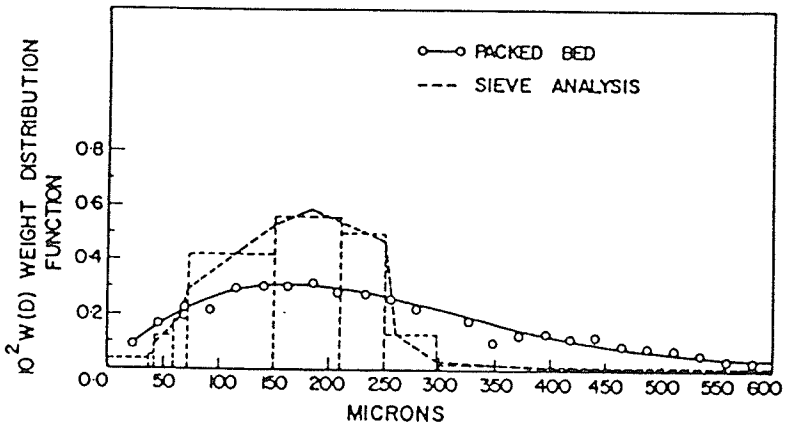


Figure 17: Comparison of results of photomicrographic work with sieve analysis (Dullien 1973)

Meyer 1983). Techniques of sample preparation, image analysis, computer graphics and optics have been developed for the quantitative analysis and reproduction of 3-D pore-structures (Lin et. al. 1983).

The most successful method of sample preparation for the image analysis of carbonate pore systems has been pore casting by epoxy resin impregnation (Rink 1973, Lin et.al. 1983, Ehrlich et.al. 1984). A discussion of this procedure is presented elsewhere.

# Chapter III

# LABORATORY INVESTIGATION

## 3.1 INTRODUCTION

The object of the laboratory study was to demonstrate basic petrographic analysis techniques for micro-porosity analysis of carbonate rock aggregates using a LEITZ TAS PLUS image analyzer. Several different carbonate aggregates of varying relative freeze-thaw durability were analyzed to assess the relevance of these porosity analysis techniques to the study of D-cracking.

One aggregate sample consisted of carbonate quarry aggregates received from the Illinois Department of Transport Materials Research section. A second sample was obtained from a previous University of Manitoba D-cracking research project. The source of this sample was the Birds Hill Esker deposit near Winnipeg which was found to be susceptible to freeze-thaw deterioration.

Sample description techniques including X-ray diffraction and SEM microscopy accompanied by a petrographic description are presented and discussed.

Specimen preparation procedures for image analysis involved pressure-injecting a blue-dyed epoxy resin compound into the inter-connected pore space of the rock micro-structure. This procedure, known as rock impregnation or pore casting, was followed by grinding and polishing to provide a 2-dimensional image of a plane passing through the porous media. Microscopic detections of the blue-dyed pore segments with a resolution down to 0.1 microns were obtained from these pore casts.

A software program written for the LEITZ image analyzer that facilitates microscopic pore segment analysis of pore casts was developed. This program analyzes the total optical porosity (TOP) of the samples and quantifies it into porosity frequency distributions called pore-complex spectra. These pore-complex spectra have been fully explained in the Image Analysis section of the literature review. Pore-complex spectra for several of the aggregate samples are presented and an analysis and critical evaluation of these techniques is presented. Details of the samples used, specimen preparation ,image analysis techniques and the results of this study are presented in subsequent sections.

## 3.2 DESCRIPTION OF AGGREGATE SAMPLES

### 3.2.1 Control Samples

One aggregate sample consisted of six 1 Kg bags of crushed carbonate quarry aggregates of known freeze-thaw durability. These samples were provided by the Illinois Department of Transport Research section. The freeze-thaw results of the aggregates, tested according to the ASTM C-666 Method B Modified test for aggregate durability, are listed in Table 6. The numbers in this table represent the elongation of the concrete test prisms after 300 test cycles. The smaller numbers correspond to a shorter prism elongation and therefore a greater freeze-thaw durability. These control samples were used primarily for the development and refinement of pore casting techniques rather than a data base for quantitative computer analysis.

While an accurate assessment of the relative freeze-thaw durability exists, in order to effectively use this data, many pore casts from each sample batch would have to be analyzed in order to correlate this data with any degree of statistical signifigance. This is due to the nature of the samples which consisted of a large batch of aggregates of varying lithology, mineralogy and size. A comprehensive analysis of this sample group is a complete research project in itself. For the pupose of this study one pore cast of each sample group was analyzed for qualitative comparison.

TABLE 6

Control Samples: Freeze Thaw Test Results (Illinios DOT)

| Code | Producer | F-T Test Result Elongation (mm) |
|---|---|---|
| FT4-103 | Specification Stone, Pana | 0.078 |
| FT4-106 | Vulcan Materials, Lehigh | 0.005 |
| FT4-108 | Columbia Quarry, Ullin | 0.191 |
| FT4-109 | Western Ill. Stone, Quincy | 0.120 |
| FT5-18C | Reed Crushed Stone | 0.076 |
| FT5-21B | Vulcan Materials, McCook | 0.015 |

### 3.2.2 Test Samples

A second sample group was chosen from the coarse carbonate fraction of aggregates which had been used for making concrete test prisms in a previous University D-cracking study. The aggregate source used in the prisms was a mineralogically heterogeneous mix of glacial gravel deposits obtained from the Birds Hill Esker Complex located 8 miles north-east of Winnipeg. The aggregate sources, code, top size and primary mineralogy is listed in Table 7. Standard petrographic aggregate test data is given in Table 8.

The prisms had been subject to as many as 300 freeze-thaw cycles of the ASTM C-666 Method B Modified test. Freeze-thaw test data for the prisms are given in Figure 18. This data

TABLE 7

Aggregate Sources (Domaschuk et.al. 1985)

| Supplier | Code | Source | Top Size | Mineralogy |
|---|---|---|---|---|
| Building Products | BP 2 | Birdshill CN Pit | 40 mm | Carbonate |
| Building Products | BP 1 | Birdshill CN Pit | 20 mm | Carbonate |
| Building Products | BP 3 | Gull Lake | 20 mm | Igneous |
| Supercrete | S1 | Ritcher | 28 mm | Carbonate |
| Supercrete | S2 | Ritcher | 14 mm | Carbonate |

TABLE 8

Standard Aggregate Test Data (Domaschuk et.al. 1985)

| Aggregate | Size | Dry Rodded un.wt. | Bulk sp.gr. | Bulk (SSD) sp.gr. | Apparent sp.gr. | Absorption (%) | Mineralogy (%) | | |
|---|---|---|---|---|---|---|---|---|---|
| | (mm) | (kg/m ) | | | | | C | Ig | O |
| BP 1 | 20 | 1710 | 2.621 | 2.674 | 2.767 | 2.02 | 75 | 23 | 2 |
| BP 2 | 40 | 1635 | 2.643 | 2.683 | 2.752 | 1.50 | 62 | 31 | 7 |
| BP 3 | 20 | 1640 | 2.614 | 2.642 | 2.689 | 1.70 | 28 | 76 | 5 |
| S 1 | 28 | 1600 | 2.620 | 2.661 | 2.733 | 1.58 | 70 | 27 | 3 |
| S 2 | 14 | 1640 | 2.566 | 2.627 | 2.743 | 2.40 | 59 | 35 | 6 |

From pebble counts
C - carbonate
Ig - igneous
O - others including cherts, volcanics and metasediments

indicated that the BP-2 aggregate source contained aggregates that were extremely susceptible to D-cracking and that the other sources contained aggregates that were less susceptible to D-cracking. This is illustrated by greater elongation of the BP-2 test prisms. This was due in part to the larger top size of this aggregate source. Because the more durable sources exhibited minor signs of deterioration this indicated that a wide range of aggregate durabilities existed within the test prisms.

In order to facilitate aggregate selection the test prisms were sectioned into 3 mm slices. Aggregates that exhibited signs of cracking were assumed to be non-durable. Individual aggregates were selected on the criteria of being either durable or non-durable. No distinction of relative durability could be assessed due to the heterogeneous nature of the sample.

#### 3.2.2.1 Non-Durable Specimens

The nondurable aggregates were selected primarily from the BP 2 aggregate source. The aggregates selected were from prisms that had to be removed from the freeze-thaw test after 150-250 cycles due to severe deterioration. In addition, two non-durable aggregate samples were obtained from the S 1 aggregate source which had revealed some deterioration. The severe cracking of the aggregate particles and the surrounding cement paste for the non-durable samples is shown in the photos in Appendix A.

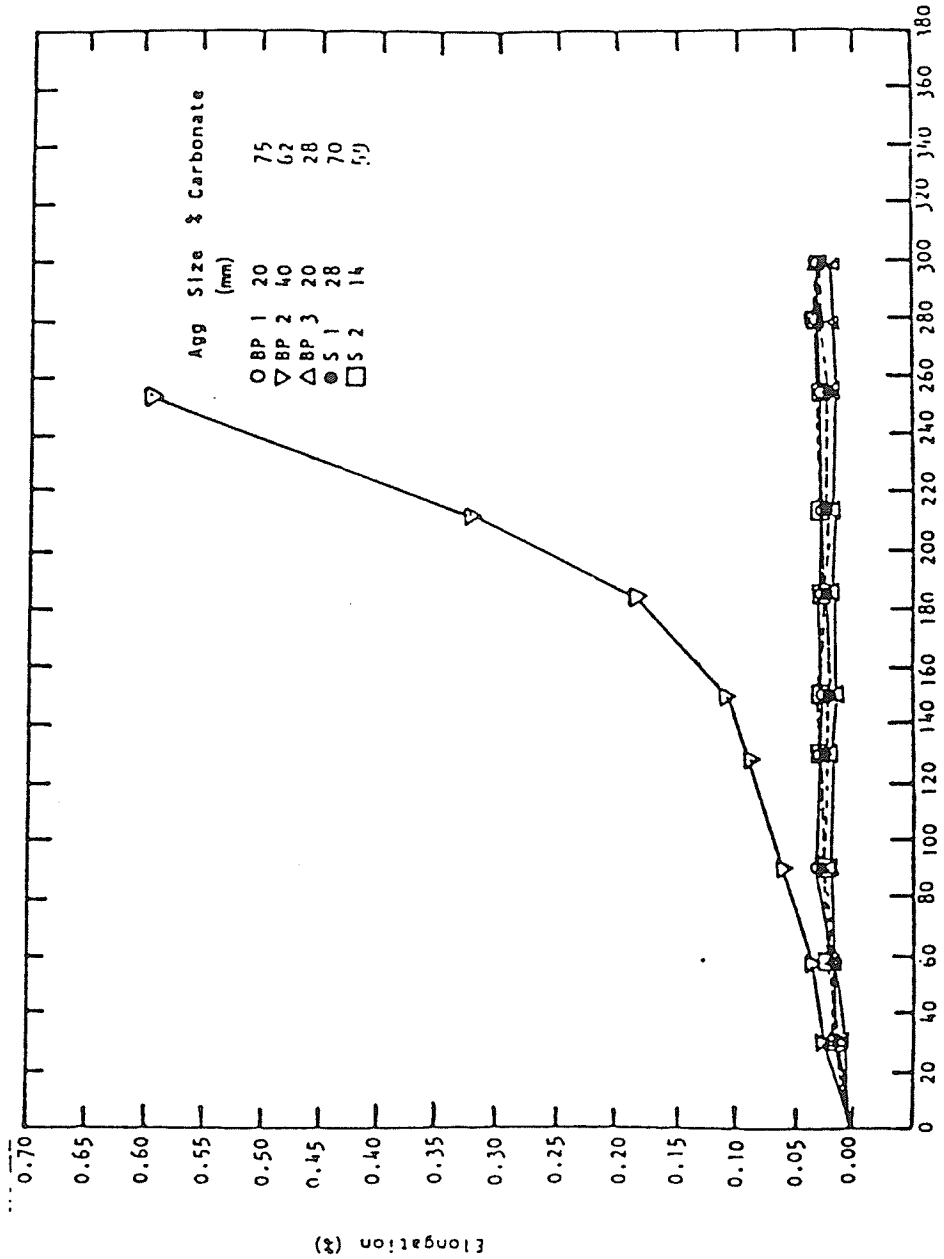


FIGURE 5 FREEZE THAW TEST DATA, FULL SCALE.

Figure 18: Test Samples: Freeze Thaw Test Results (Domaschuk et.al. 1985)

### 3.2.2.2 Durable Specimens

All of the durable aggregates were selected from the S 1 aggregate source. These aggregates revealed no evidence of deterioration after being subjected to 300 freeze-thaw cycles and therefore were assumed to be durable. There is some uncertainty regarding the assessment of durability of this sample group. While the prisms exhibited no visual signs of deterioration after 300 F-T cycles, this does not necessarily mean that they would not show deterioration with additional testing. Also this aggregate source was of smaller top size which is known to increase freeze-thaw durability. It is possible that the durable sample group contained some aggregates of marginal durability. Prism sections containing the durable aggregates are illustrated in the photos in Appendix A.

## 3.3 X-RAY DIFFRACTION

Rock mineralogical identification using x-ray diffraction is a very important component of a comprehensive petrographic sample description for the identification of D-cracking susceptible aggregates.

A small portion of each of the aggregate samples was ground into a fine powder and spread evenly on a glass slide for X-ray diffraction analysis. Each slide was analyzed at

40 KV and 40 MA with nickel-filtered Cu K-alpha radiation on a Philips model PW1729 x-ray diffractometer. The operating conditions consisted of a time constant of 0.5 and a scalar equal to 2000. All samples were run at medium speed (6 degrees 2-theta/min) and scanned 3 times from 28 to 32 2-theta. This allowed for average intensity measurements of the principle calcite (3.03 A ) and dolomite (2.88 A) reflections. The percent of dolomite by weight was calculated using the dolomite/(dolomite+calcite) ratio and a standard calibration curve (Figure 19). The results of this test for all of the specimens analyzed are listed in Table 9.

This data indicated that rock type mineralogy of the samples included limestone, dolomitic limestone, calcitic dolomite, dolomite, silicified limestone and silicified dolomite.

No apparent correlation existed between mineralogic composition as obtained from x-ray diffraction peak height analysis, and D-cracking susceptibility for the carbonate rock aggregates investigated.

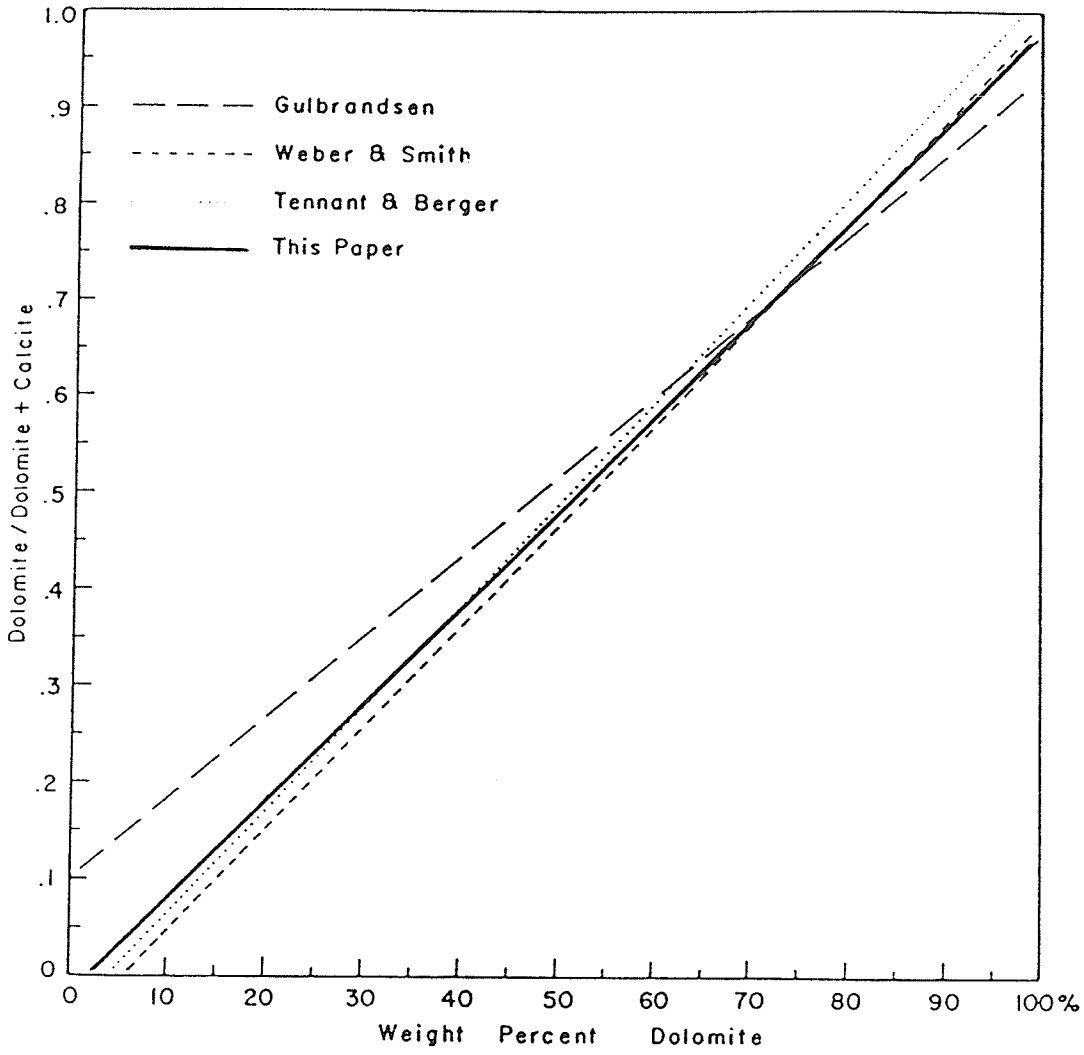


Figure 19: Weight Percent Dolomite Calibration Curve (Royse et.al. 1971)

TABLE 9

X-ray Diffraction Data

| Sample No. | Dolomite Intensity | Calcite Intensity | Do Do + Ca | Dolomite Weight % |
|---|---|---|---|---|
| Control Samples | | | | |
| FT4 103 | 0 | 10447 | 0.0 | 0 % |
| FT4 106 | 12158 | 0 | 1.0 | 100 % |
| FT4 108 | 204 | 9687 | 0.021 | 4 % |
| FT4 109 | 527 | 8686 | 0.057 | 7 % |
| FT5 18C | 298 | 13581 | 0.021 | 4 % |
| FT5 21B | 8017 | 0 | 1.0 | 100 % |
| Durable Test Samples | | | | |
| S 1-11 | 13061 | 152 | 0.99 | 100 % |
| S 1-12 | 15668 | 321 | 0.98 | 99 % |
| S 1-13 | 14168 | 0 | 1.00 | 100 % |
| S 1-14 | 304 | 8311 | 0.04 | 6 % |
| S 1-15 | 8908 | 217 | 0.98 | 99 % |
| S 1-16 | 4437 | 3638 | 0.55 | 57 % |
| S 1-17 | 13454 | 0 | 1.00 | 100 % |
| S 1-18 | 13369 | 210 | 0.98 | 99 % |
| S 1-19 | 4102 | 216 | 0.95 | 98 % |
| S 1-20 | 1979 | 7410 | 0.21 | 23 % |
| S 1-21 | 12975 | 149 | 0.99 | 100 % |
| Non-Durable Test Samples | | | | |
| BP 2-1 | 9434 | 212 | 0.97 | 99 % |
| BP 2-2 | - | - | - | - |
| BP 2-3 | 12093 | 97 | 0.99 | 100 % |
| BP 2-4 | 13642 | 108 | 0.99 | 100 % |
| BP 2-5 | 12380 | 164 | 0.99 | 100 % |
| BP 2-6 | 4197 | 3322 | 0.56 | 58 % |
| BP 2-7 | 8541 | 2807 | 0.75 | 78 % |
| BP 2-8 | 13948 | 78 | 0.99 | 100 % |
| BP 2-9 | - | - | - | - |
| S 1-9 | 1309 | 7198 | 0.15 | 17 % |
| S 1-10 | 8604 | 284 | 0.97 | 99 % |

## 3.4 SCANNING ELECTRON MICROSCOPE (SEM)

Small fragments, approximately 6 mm in diameter, of each aggregate specimen were obtained for SEM analysis. The fragments were washed in an ultrasonic bath, mounted on small base sample holders and a thin (100 A) film of gold was applied with a Balzer sputter-coater.

The samples were individually analyzed using a Cambridge Sterioscan Mark II scanning electron microscope. Numerous photographs of varying magnifications of each specimen were taken to obtain a 'representative' view of the rock microstructure.

SEM micrographs provided useful qualitative information of the carbonate rock aggregates analyzed. Grain morphology, texture and porosity types, described in Appendix B, provided a concise visual evaluation of the rock mineralogy and associated pore structure type. In most cases SEM photo description corresponded favorably with XRD data.

SEM photos exhibited mineral grain structure representative of pore casts images at the same magnification. Porosity estimations interpreted from the SEM micrographs underestimated porosity evaluations obtained from pore cast images by as much as 20% (TOP). These findings were not unexpected due to the 3-D nature of the SEM mineral grain structure images and the finite size of the sample area analyzed.

SEM was not incorporated in the image analysis computer analysis due to the complex nature of the images. Special sample preparation procedures are required to facilitate such procedures. Scanning Electron Microscopy provides a feasable method for accurate mineralogical identification when used in conjunction with XRD analysis. SEM is another fundamental component of a comprehesive petrographic description for the identification of D-cracking susceptible concrete aggregates. A comprehensive petrographic description of the SEM micrographs for all of the carbonate rock samples, provided by Laramide Petrographic Services, is presented in Appendix B. The SEM micrographs for all rock samples are located in the 'Sample Image Files' (Appendix E).

## 3.5 PORE CASTING

Pore casts of several carbonate rock samples analyzed in this study were obtained using a rock impregnation technique developed at the University of Calgary (McKellar et.al. 1981). The basic procedures for this technique were:

1. A small fragment of each specimen (diameter < 20mm) to be analysed was obtained.
2. Each fragment was washed thoroughly in an ultrasonic bath and then air dryed.
3. The fragment was then placed in a 30 ml plastic micro-beaker marked with the sample ID#.

4. The epoxy resin-hardener compound was then mixed according to specifications (see Appendix C) with a small quantity of blue dye added.

5. The epoxy compound was then poured into the beakers containing the specimen fragments. In this investigation 6 samples were cast at a time.

6. The beakers were then placed in a vacuum bell jar and were subjected to a vacuum to evacuate the pores (about 10-15 min).

7. When the bubbling stopped, the bell jar was allowed to come to atmospheric pressure and the beakers were removed and placed into the pressure bomb.

8. Once properly in place in the pressure bomb, the samples were subject to a vacuum pressure for an additional 20-30 minutes.

9. At this point the vacuum was turned off andpressure from a nitrogen bottle applied gradually. A pressure of 2000 psi was sustained for about 20-30 min.

10. After this pressure impregnation period the pressure was gradually reduced to atmospheric.

11. The rock fragments were then centered in the beaker with a toothpick and placed in the fume hood to cure (16-24 hours).

12. The samples were then ready to be ground down, sanded and polished to expose the rock surface.

Details of these procedures are presented in Appendix C.

Both red and blue dyes were used in the pore casting procedures. The blue dye was found to provide greater optical recognition characteristics when viewed under the LEITZ microscope. The pore casting apparatus used to impregnate the pore cast specimens and the fume hood are illustrated in Figure 20. Figure 21 illustates two pore cast plugs of rock samples produced subsequent to grinding, sanding and polishing down to 0.25 microns.

The pore complex analysis of the carbonate rock aggregate specimens in this study was carried out using reflected light microscopy on polished pore plug sections. The procedures used provided an excellent method for a 2-dimensional analysis of pore segments contained in the pore structure of carbonate aggregates. The quality of the pore cast images produced were of very high quality which provided high resolution images using the LEITZ computer microscope.

Carbonate rocks by nature are very soft and susceptible to scratching during polishing procedures. Care was taken during polishing procedures to minimize this scratching which can drastically affect the quality of the images produced. Polishing down to 0.25 microns was required to ensure a quality finish on the pore cast specimens. When scratches still remained after these steps were taken, they were eliminated from grey level detection by increasing the lamp adjustment on the microscope. Another excellent method for microporosity detection is accomplished using a Rhoda-

mine B flourescent dye and flourescent microscope light attachment. However the necessary resources to implement these procedures were not readily available. Directions for the use of this dye are included in Appendix C. This method has proven to be very useful for the detection of microporosity in thin sections.

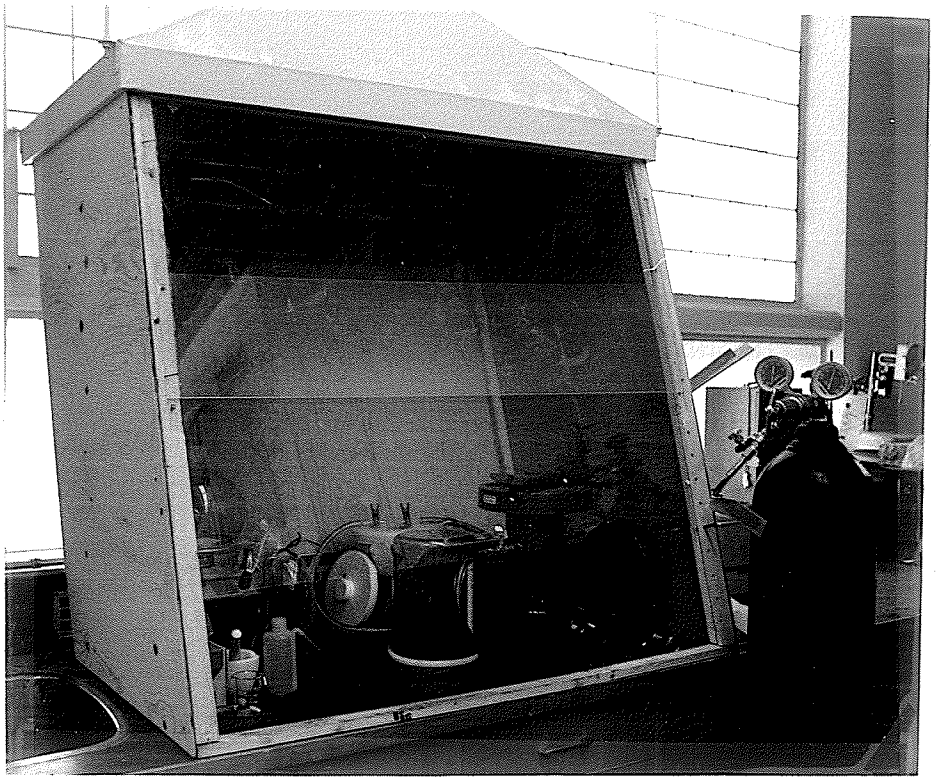

Figure 20: Pore Casting Apparatus

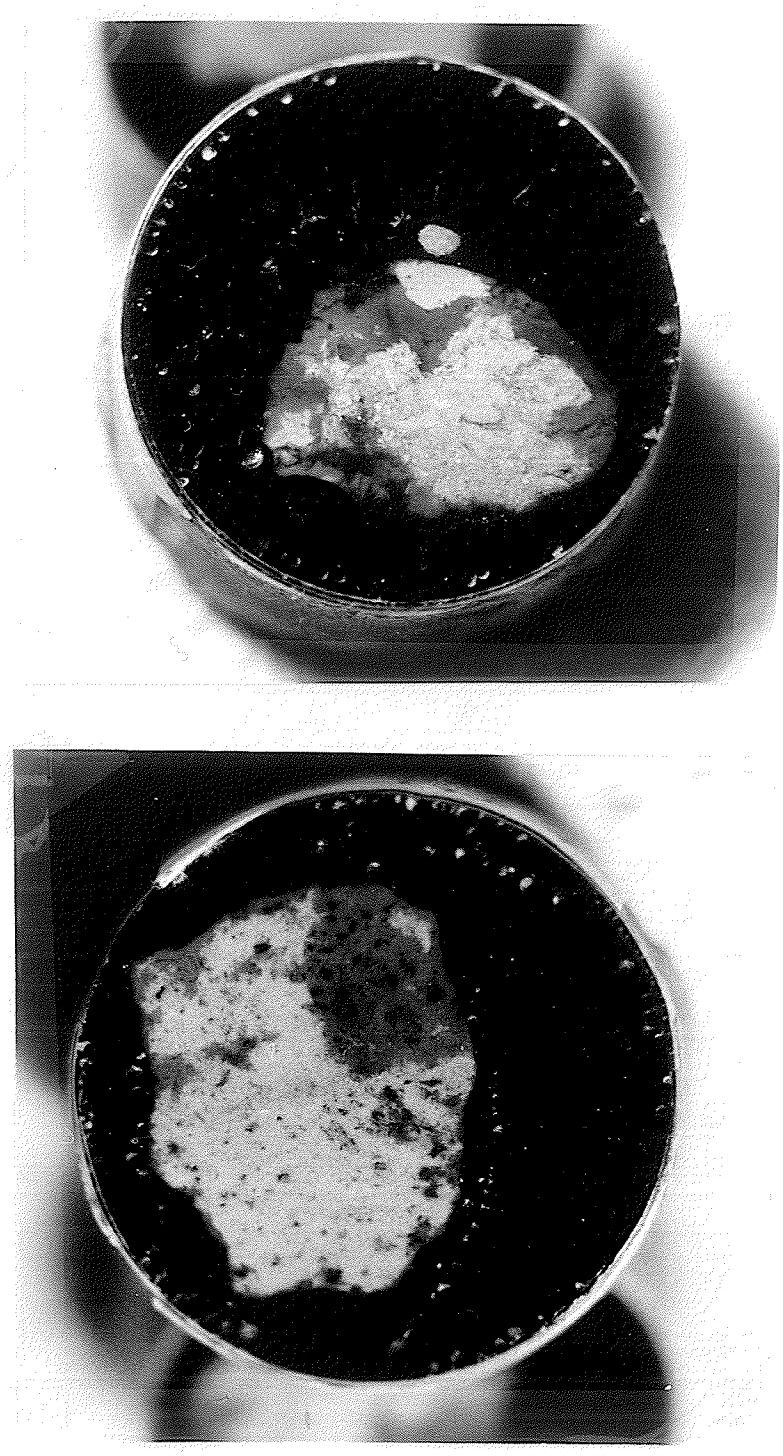

Figure 21: Pore Cast Samples (Plug diameter = 25mm)

## 3.6 COMPUTER ANALYSIS

The LEITZ TAS PLUS imge analysis computer is a fully programable computer system developed for the automatic pro-

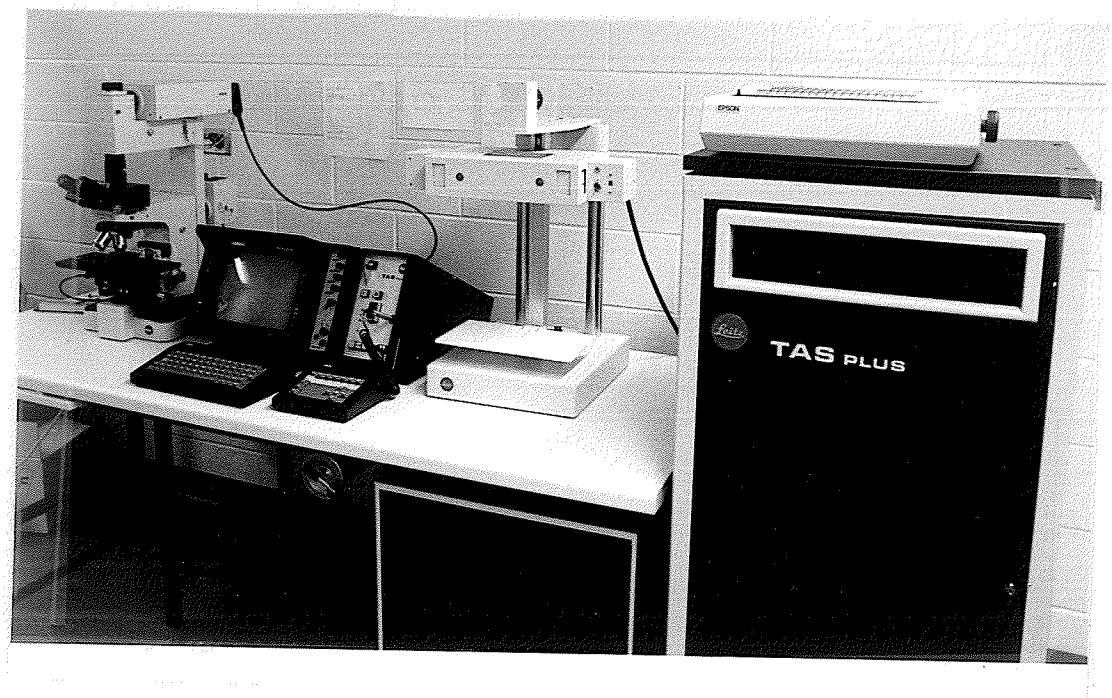


Figure 22: Image Analysis Computer

cessing and quantification of optical images (Figure 22). A comprehensive explanation of the operation of this system has been presented in a previous section. For the purpose of this study a program was synthesized to facilitate micro-porosity analysis of polished sections of blue-dyed carbo-nate rock pore casts. The algorithm for this program was adopted from Petrographic Image Analysis (PIA) techniques developed at the University of South Carolina (Ehrlich et.al. 1985). A printout of the computer program developed,

written in TASIC (a language similar to Fortran), is listed in Appendix D.

The micro-porosity analysis program calculated the total optical porosity (TOP) of the inter-connected pore space of the rock mico-structure. Each bitplane was represented by ten randomly spaced fields of view. An example bitplane image of a pore cast viewed on the LEITZ computer microscope is illustrated in Figure 23. This image consists of a 512 X 512 pixel array. The field of view in this image is 182.5 microns which corresponds to a magnification of 1280X. This magnification allowed for the detection of micro-porosity down to 0.3 microns which corresponds to 1 pixel. However pore geometry can only be determined when a pore is expressed over a minimum of 4 to 8 pixels. At higher magnifications resolution of larger pores within a field of view became very distorted and undetectable. Focusing, lighting and detection problems also became appreciable at these magnifications making them unacceptable. For these reasons a magnification of 1280X was found to be optimum for the investigation of the microstructure of carbonate rock pore casts. All samples were analyzed at the same magnification to facilitate qualitative and quantitative comparisons.

A sample 'pore-complex spectra' produced by this program extracted from the image in Figure 23 is given in Figure 24. This printout includes the number of frames analyzed, total optical porosity (TOP) and the total, pore, roughness and number frequency distributions.

BITPLANE IMAGE: 1.
FIELD WIDTH: 182.5 MICRONS

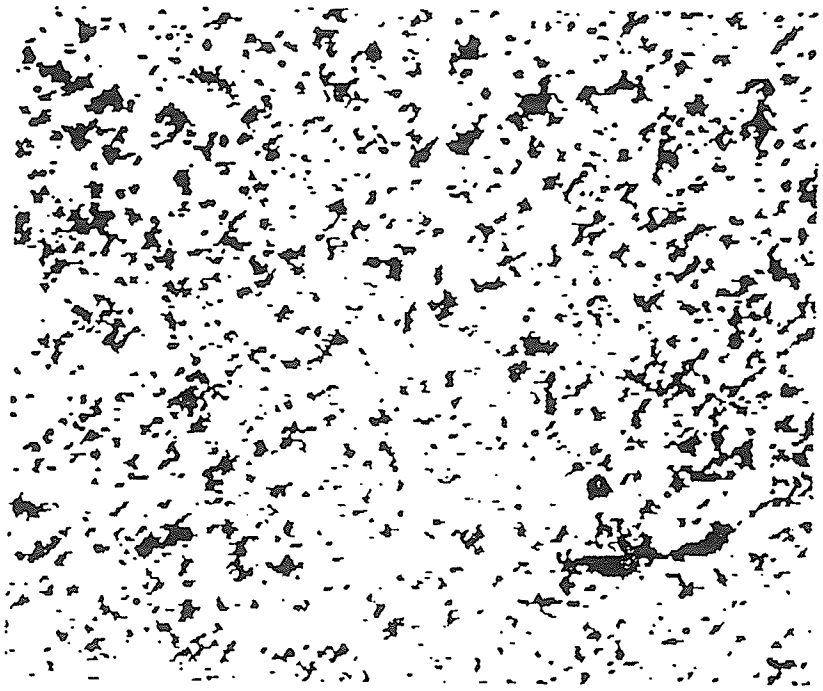

Figure 23: Computer Image of Pore Cast

PORE STRUCTURE ANALYSIS OF CARBONATE ROCK AGGREGATE PORE CASTS
POROSITY ANALYSIS
PORE COMPLEX SPECTRA

SAMPLE #: S1-10
# OF FRAMES: 10.

TOTAL OPTICAL POROSITY
>>>19.39% <<<

TOTAL POROSITY

| % POROSITY | E/D CYCLES | |
|---|---|---|
| 53.3180 | 1.00000 | +----------* |
| 35.1449 | 2.00000 | +-------* |
| 7.73346 | 3.00000 | +--* |
| 1.56172 | 4.00000 | * |
| 0.537981 | 5.00000 | * |
| 0.894250E-01 | 6.00000 | * |
| 0.000000 | 7.00000 | * |

PORE POROSITY

| % POROSITY | E/D CYCLES | |
|---|---|---|
| 30.3901 | 1.00000 | +----------* |
| 28.8787 | 2.00000 | +---------* |
| 6.87355 | 3.00000 | +--* |
| 1.45727 | 4.00000 | * |
| 0.514372 | 5.00000 | * |
| 0.894250E-01 | 6.00000 | * |
| 0.000000 | 7.00000 | * |

ROUGHNESS POROSITY

| % POROSITY | E/D CYCLES | |
|---|---|---|
| 22.9279 | 1.00000 | +----------* |
| 6.26619 | 2.00000 | +--* |
| 0.859910 | 3.00000 | * |
| 0.104448 | 4.00000 | * |
| 0.236082E-01 | 5.00000 | * |
| 0.000000 | 6.00000 | * |
| 0.000000 | 7.00000 | * |

NUMBER FREQUENCY

| # OF PORES | E/D CYCLES | |
|---|---|---|
| 9575.00 | 1.00000 | +----------* |
| 2589.00 | 2.00000 | +---* |
| 311.000 | 3.00000 | * |
| 40.0000 | 4.00000 | * |
| 8.00000 | 5.00000 | * |
| 1.00000 | 6.00000 | * |
| 0.000000 | 7.00000 | * |

Figure 24: Pore-Complex Spectra

### 3.6.1 Sample Analysis

Twenty-six of the twenty-eight samples were analyzed using the 'Pore-Complex Spectra' program on the LEITZ TAS PLUS image analyzer. The Total Optical Porosity (TOP) for all of the specimens is illustrated in the bar graph in Figure 25. The sample groups have been separated and plotted in ascending order of porosity. This plot illustrates that the non-durable specimens exist in a narrower range of TOP than the durable specimens. TOP ranged from 15.1% to 23.4% for the non-durable specimens, 5.2% to 22.4% for the durable specimens and 3.2% to 22.5% for the control specimens. One of the durable specimens recorded a porosity of 39.0% but it is felt this high estimate was a direct result of program algorithm and did not accurately represent the true porosity. This carbonate rock type is also a special case and its occurance is rare. For these reasons this specimen was eliminated from subsequent analysis. Special adjustments to the computer algorithm would have to be made to facilitate the analysis of this type of pore structure at the same magnification.

Figures 26 to Figure 28 further illustrate the TOP of the individual sample groups divided into 'pore' and 'roughness' porosity. Analysis of the proportions of pore and roughness porosities did not indicate any correlations with D-cracking susceptibility. A meaningful interpretation of this data was not possible due to the nature of the basic algorithm

used for porosity analysis and the uncertainty of relative specimen durabilities.

Figure 29 and Figure 30 illustrate the percentage of the 1 E-D 'pore porosity' of the non-durable and durable sample groups respectively. Analysis of this data indicates that the non-durable sample group, with the exception of one sample, had a higher absolute percentage of 1 E/D pore porosity (< 0.3 micron pores) than did the durable sample group. This was consistent with the findings discussed in the Literature Review section of this paper.

The algorithm used to calculate the pore porosities tended to overestimate the roughness porosity portion of pore segments by oversimplification. This resulted in the pore-complex spectra being weighted towards the roughness porosity proportion especially when analyzing larger pores. Occurences such as pore separation (when a pore splits into two or more segments) also resulted in significant overestimation of roughness porosity. When a portion of a split segment disappeared it was registered as roughness porosity rather than part of the pore porosity.

The computer memory space alloted for program and parameter storage limits the usefulness of LEITZ TAS PLUS for use in the developement of Petrographic Image Analysis procedures. These techniques require a much larger memory capacity for data manipulation and processing than was available.

Computer interfacing involving the direct transfer of image data to a microcomputer for data processing would solve this problem and allow for the continued development of these techniques.

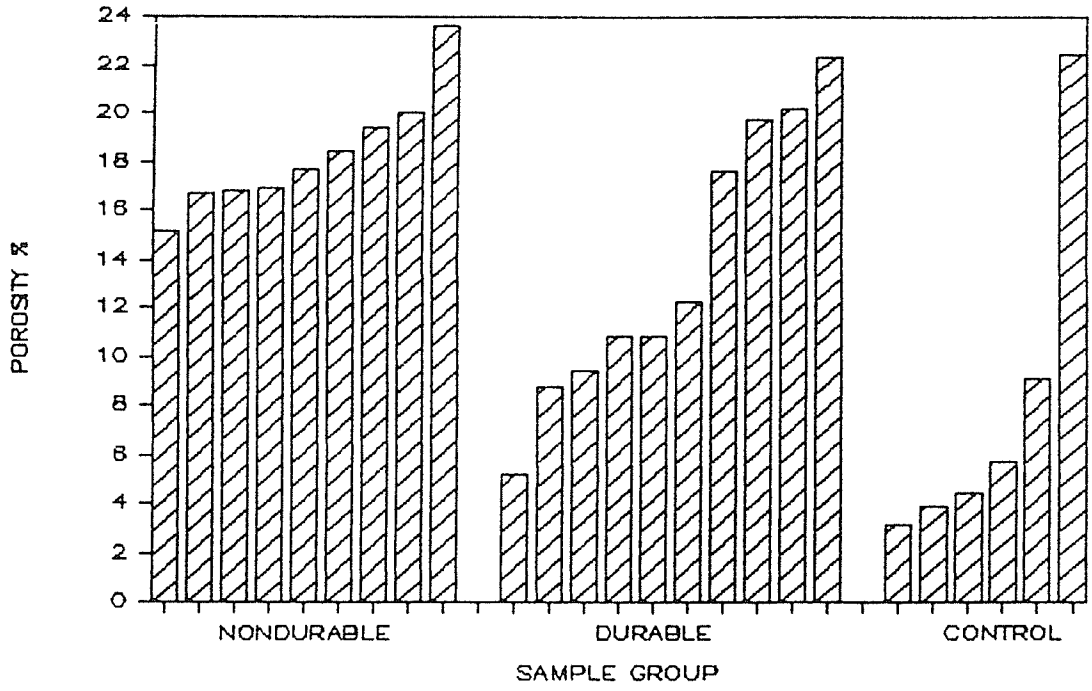


Figure 25: Total Optical Porosity: All Samples

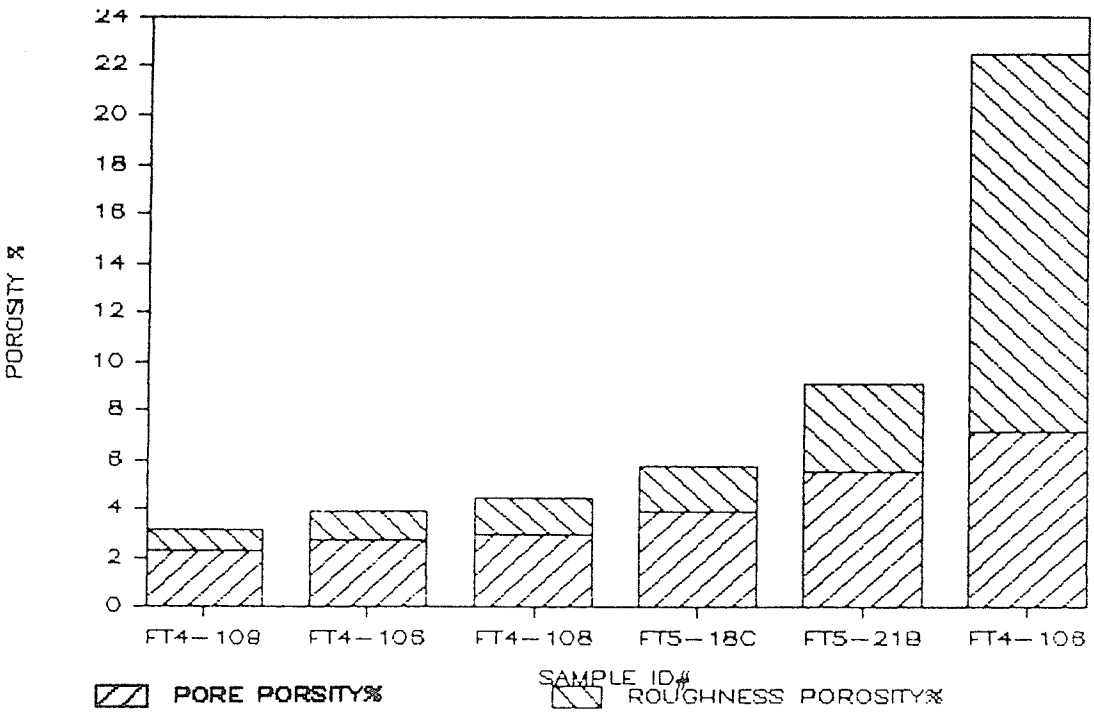


Figure 26: Total Optical Porosity: Control Sample

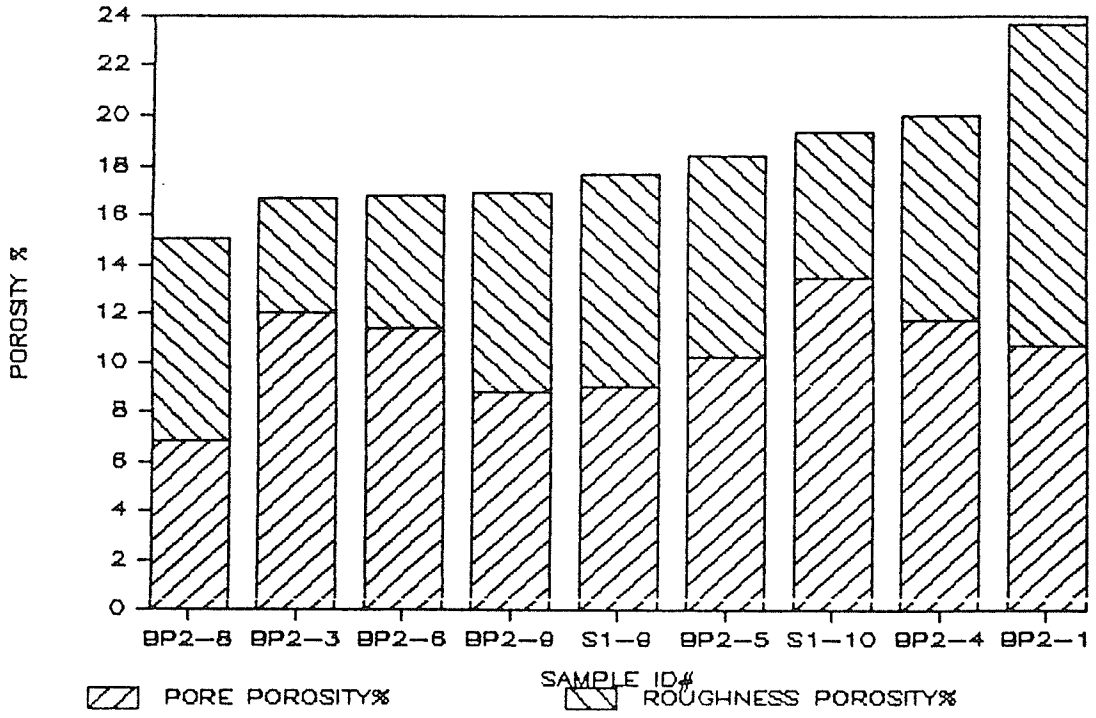


Figure 27: Total Optical Porosity: Non-Durable Sample

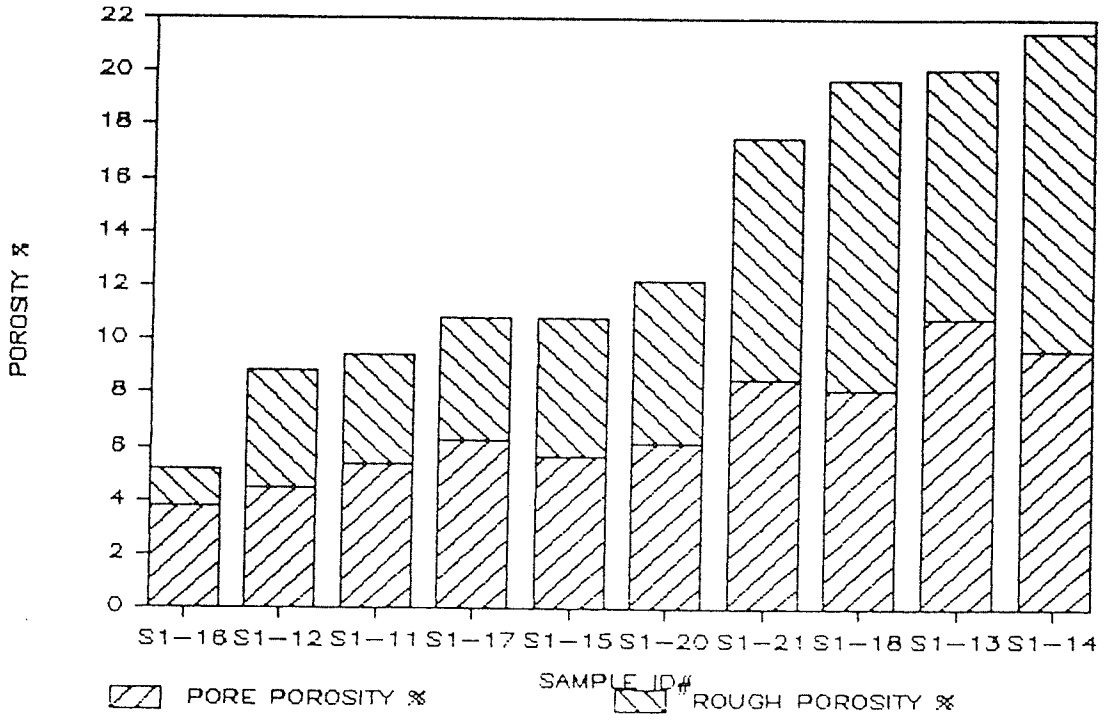


Figure 28: Total Optical Porosity: Durable Sample

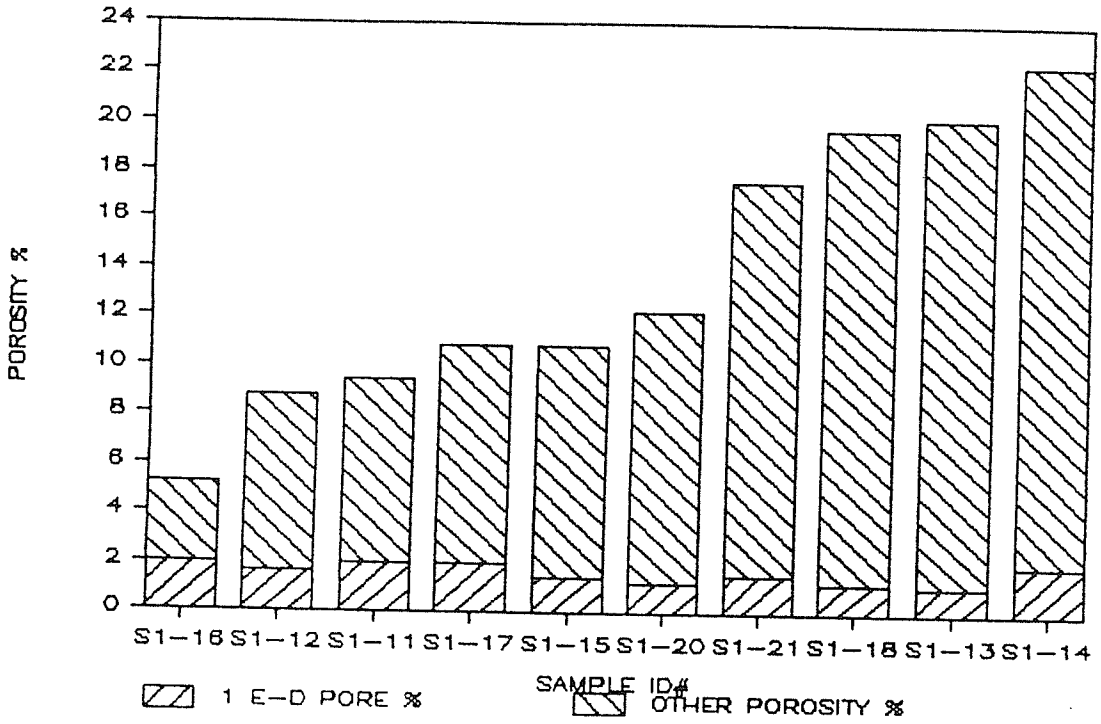


Figure 29: 1 E-D Pore Porosity: Non-Durable Sample

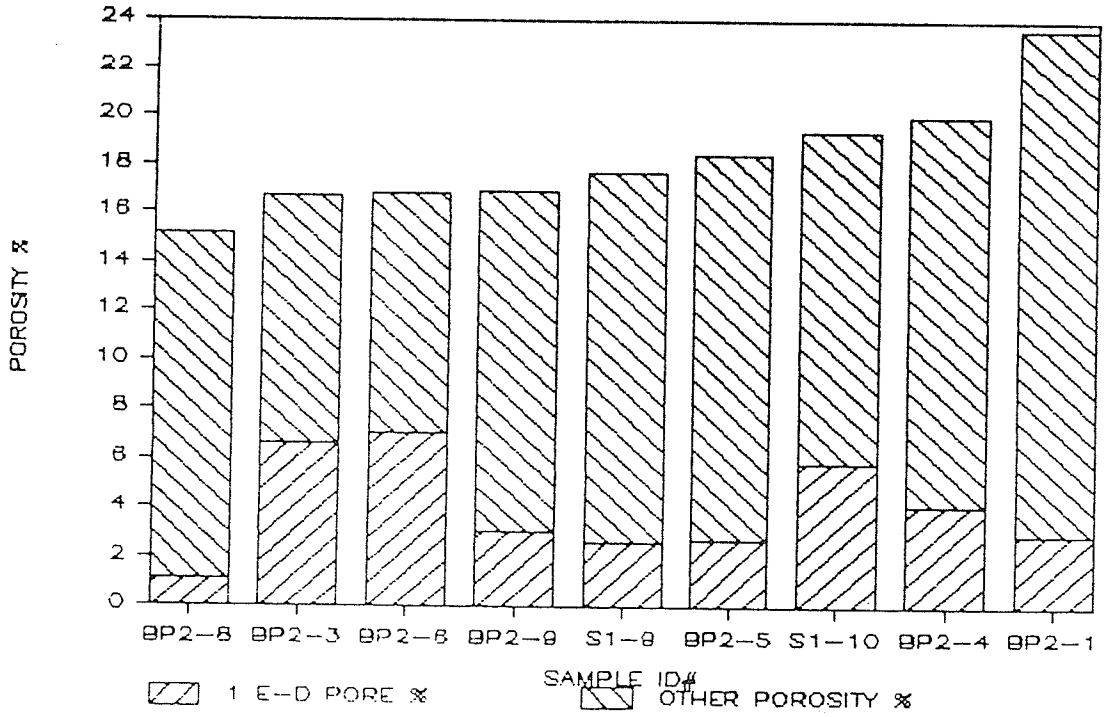


Figure 30: 1 E-D Pore Porosity: Durable Sample

# Chapter IV

# SUMMARY AND RECOMMENDATIONS

## 4.1 SUMMARY

This thesis dealt with the investigation of D-cracking of portland cement concrete pavements. This phenomenon has been attributed to the freeze-thaw deterioration of certain types of carbonate aggregates. The primary objective of this thesis was to develop and assess techniques of porosity analysis for carbonate rock aggregates, relevant to the study of D-cracking.

In the first section a literature review of standard engineering and geological techniques of pore systems analysis used for the evaluation of carbonate rock aggregate porosity was presented. This section illustrated the general lack of reliable standard tests for the evaluation of carbonate rock aggregate properties. While these tests provide a good general index for aggregate investigations they were found to be inadequate for the identification of D-cracking susceptible aggregates.

The review included pore systems analysis techniques collectively referred to as Petrographic Image Analysis (PIA). These techniques have been used to quantitatively evaluate

physical properties of carbonate pore complexes such as porosity, permeability and pore-size distribution, accurately and concisely. The review was based on information obtained from computer searches of GEOREF, Engineering Index and the PCA bibliography data base library systems.

The findings of the review were used to develop suitable procedures of porosity analysis to assist in the identification of local D-cracking susceptible aggregates. The porosity analysis procedures developed included specimen identification, preparation and analysis. The specimen identification consisted of X-ray diffraction and Scanning Electron Microscopy along with a comprehensive petrographic description. Specimen preparation involved a technique known as pore casting. The purchase and assembly of the apparatus necessary for implementing this procedure comprised a major portion of this study. This included the design and fabrication of pore cast system components including a high-pressure vessel and connections, a vacuum vapour trap and a fume hood set up. The adaptation of a basic Petrographic Image Analysis algorithm to the operation and programming language of the LEITZ TAS PLUS computer system was another major portion of this investigation.

Twenty-six specimens were analyzed using a simplified 'Pore-Complex Spectra' program developed for the LEITZ computer system. Total Optical Porosity (TOP) ranged from 15.1% to 23.4% for the non-durable specimens and from 5.2%

to 22.4% for the durable specimens. This data indicated that the non-durable aggregates tested in this study existed in a narrower range of TOP than did the durable aggregates. The non-durable sample also exhibited narrower pore-size ranges than the durable sample.

The non-durable sample had a higher absolute percentage of 1 E/D pore porosity (< 0.3 micron pores) than the durable sample. This finding is consistent with findings discussed in the literature review section of this thesis. Analysis of the 'pore' and 'roughness' porosity partition was inconclusive due to the nature of the samples.

The findings of this preliminary study indicate that a relationship between parameters obtained through PIA techniques and the D-cracking susceptibility of carbonate aggregates may exist.

The complex data storage and manipulation requires a more comprehensive analysis of the various parameters such as size, shape, density, orientation and distribution which is beyond the capabilities of the LEITZ TAS PLUS. Computer interfacing between the LEITZ computer system and a connected micro-computer system would provide a means for processing the large data base associated with Petrographic Image Analysis.

## 4.2 RECOMMENDATIONS

Further research into Petrographic Image Analysis techniques for the study of D-cracking is required. This research should involve interfacing the LEITZ TAS PLUS image analyzer with a micro-computer. Using the LEITZ computer for image data aquisition and the interfaced computer for data processing would provide a means to further develop Petrographic Image Analysis techniques at the University of Manitoba. Specifically this would require:

1. Modifications to the existing pore complex analysis algorithm.

2. Interfacing the LEITZ TAS PLUS with an IBM PC/XT or compatable to allow one way data transfer from the LEITZ computer to the interfaced computer.

3. Development of a simple pore classification algorithm. This algorithm would separate pores into the classifications of rounded, rounded with convoluted edges, elongated and elongated with branches.

4. Investigation of relevant data analysis and processing techniques consistent with established PIA procedures. This would include programming to allow analysis of various parameters or combinations of parameters selected by the operator.

## REFERENCES


Alford,N.M. and A.A. Raham. 1981. An assesment of porosity and pore-sizes in hardened cement paste. Jr. Mat. Science.16:3105-3114.

Aschenbrenner B.C. et.al. 1972. Teodorvich's method for determining permeability from pore-space characteristics of carbonate rocks. AAP6 Repr. Ser.#5: 82-85.

Brunauer,S.,Skalny,J. and I. Odler. 1973. Complete pore-structure analysis. Proc. Int. Sym. RIEM/IUPAC Prague. vol.1,C:3-26.

Brown,R.H. 1968. Pore studies of carbonate aggregates by an evaporation technique. Ph.D. Thesis, Purdue University.

Choquette,P.W. and L.C. Pray. 1970. Geologic nomenclature and classification of porosity in sedimentary carbonates. AAPG Repr. Ser 5:154-197.

Cebeci,O.Z.,Demirel,T. and R.A. Lohnes. 1978. Evaluation of hysterisis in mercury intrusion porosimetry by second- intrusion method. Trans. Res. Rec. No. 675:15-20.

Dolch,W.L. 1978. Porosity. ASTM Special Technical Publ. 169B:646-656.

Domaschuk L., Ganapathy G. and G. Hermanson. 1985. D-cracking of concrete pavements in Manitoba. Civil Engineering Dept., University of Manitoba; Transport Canada Winnipeg: Report.

Dullien,F.A.L. 1973. Photomicrographic pore-size distributions using quantitative stereology and application of results in tertiary petroleum recovery. Proc. Int. Sym. RILEM/IUPAC Prague. 1C:173-186.

Dunn,J.R. and P.P. Hudec. 1972. Frost and sorption effects in argillaceous rocks. Hwy. Res. Rec. No.393:65-78.

Ehrlich R., Kennedy S.K., Crabtree S.J. and Cannon R.L. 1984. Petrographic Image Analysis; I. Analysis

of reservoir pore complexes. Jour. Sed. Pet. Vol 54 No 4:1365-1378.

Eyraud,C.,et. al. 1973. Determination calorimetrique de la distribution des rayons de pores. Proc. Int. Sym. RILEM/IUPAC Prague. 1C:81-99.

Fischmeister,H.F. 1973. Determination of pore-structure by stereological measurements. Proc. Int. Sym. RILEM/IUPAC Prague. 6C:439-476.

Folk,R.L. 1962. Spectral subdivision of limestone types. Classification of Carbonate Rocks-A Symposium. AAPG (Memmoir 1):62-84

Gilliot,J.E. 1980. Properties of aggregates affecting concrete in North America. Q.J. Eng. Geol. 13,4:289-303.

Girard,R.J.,Myers,E.M.,Manchester,G.D. and W.L. Trimm. 1982. D-Cracking:pavement design and construction variables. Trans. Res. Rec. 853:1-9.

Gribanova,E.V. and O.N. Grigorov. 1973. Some peculiarities of capillary rise of moisture in porous medium. Proc. Int. Sym. RILEM/IUPAC Prague. 6C:342-350.

Harvey R.D. and J.C. Steinmetz. 1972. Petrography of carbonate rocks by image analysis. Forum on Geology of Industrial Minerals, 7th Proceedings:161-170.

Hesse,D. 1973. Pore-structure determination of porous media from diffusion measurement. Proc. Int. Sym. RILEM/IUPAC Prague. 1C:139-153.

Hilliard,J.E. 1972. Stereology-an experimental viewpoint. Proceedings of the Symposum on Statistical and Probabilistics Problems in Metallurgy. Applied Probability Trust:92-111.

Hiltrop,C.L. and J. Lemish. 1959. Relationship of pore-size distribution and other rock properties to serviceability of some carbonate aggregates. Physical and chemical properties of cement and aggregates in concrete. H.R.B Bull. 239:1-23.

Hugman,R.H.H. and M. Friedman. 1979. Effects of texture and composition on mechnical behavior of experimentally deformed carbonate rocks. A.A.P.B. 63(9):1478-1489.

Kaneuji,M.,Winslow,D.n. and W.L. Dolch. 1980. The relationship between an aggregates pore-size distri-

bution and it's freeze-thaw durability in concrete. Cement and Concrete Research. 10:433-441.

Larson,T.,Cady P.,Franzen,M. and J. Reed. 1964. A critical review treating methods of identifying aggregates subject to destructive volume change when frozen in concrete and a proposed program of research. Hwy. Res. Bd. Special Report 80.

Larson,T.D.,Boettcher,A.,Cady,P.D.,Franzen and J.R. Reed. 1965. Identification of concrete aggregates exhibiting frost susceptibility. NCHRP Report. 15.

Lin,C. and J. Hamanski. 1983. Pore geometry: a new system for quantitative analysis and 3-D display. Journal of Sedimentary Petrology. 53(1):670-672.

Lindgren,M.N. 1980. The prediction of freeze-thaw durability of course aggregate in concrete by mercury intrusion porosimeter. MSc. Thesis, Dept. of Civil Eng.,U. of Purdue.

Litvan,G.G. 1973. Pore-structure and frost susceptibility of builing materials. Proc. Int. Sym. RILEM/IUPAC Prague. 2F:17-30.

Litvan,G.G. 1978. Absorption systems at temperatures below the freezing point of the absorbtive. CNRC Rep 183. 4:283-302.

Litvan,G.G. 1981. Frost action in porous systems. Div. of Bldg. Res. Paper. no. 1176.

Martin,R.B. 1973. Equivalence of porosity and specific surface measures in one,two and three dimesions. Proc. Int. Sym. RILEM/IUPAC Prague. 1A:35-52.

McKellar M.J. and N.C. Wardlaw. 1981. Rock Impregnation. Department of Geology and Geophysics Report; University of Calgary.

Meyer,L.P.H. 1983. Determination of air content of hardened concrete using image analysis. MSc thesis,U. of Windsor.

Ministr,Z. 1973. Stereology and mercury porosimetry. Proc. Int. Sym. RILEM/IUPAC Prague. 1C:155-171.

Mysyk,W.K. and R.J. Edwards. 1985. Minerological analysis and littertature review of limestone aggregate porosity/permeability from Apron I,Winnipeg International Airport, Winnipeg, Manitioba. Tansport Canada Report.

Nazare,S. and G.Ondrocek. 1973. Characteristics of microstructure and it's effects on the properties of porous materials. Proc. Int. Sym. RILEM/IUPAC Prague. 6C:477-495.

Petruk,W. 1982. Image analysis in process mineralogy. Process Mineralogy; II, Applications in Metallurgy, Ceramics and Geology. Am. Inst. Min., Metall. and Pet. Eng. New York, N.Y.:39-53.

Pittman,E.D. and R.W. Duschatko. 1970. Use of pore casts and scanning electron microscope to study pore geometry. Jour. Sed. Pet. 40:1153-1157.

Pittman,E.D. and J.B. Thomas. 1979. Some applications of SEM to the study of reservoir rock. Jour. Pet. Tech. 31(11):1375-1380.

Racic,D. 1984. An investigation of the effect of super plasticisers on the entrained air void system using image analysis. MSc Thesis, U. of Windsor.

Ravaglioli,A. and G. Vecchi. 1973. Assesment of the frost resistance of ceramic bodies by means of porosity meter tests. Proc. Int. Sym. RILEM/IUPAC Prague. 4F:117-128.

Rink,M. 1973. An image analysis procedure for digital computers and it's application to investigations on pore-structures. Proc. Int. Sym. RILEM/IUPAC Prague. 6C:495-505.

Rink M. and J.R. Schopper. 1976. Pore-structure and physical properties of porous sedimentary rocks. Pure Appl. Geophys. 114:273-284.

Rink M. and J.R. Schopper. 1978. On the application of image analysis to formation evaluation. Log Anal. Vol. 19. No. 1:12-22.

Robinson,R.B. 1972. Classification of reservoir rocks by surface texture. AAPG Repr. Ser. 5:95-107.

Royse C.F.Jr., J.S. Wadell and L.E. Peterson. 1971. X-ray determination of calcite-dolomite: An evaluation. Jour. Sed. Pet. Vol. 41 No. 2:483-488.

Sing,K.S.W. 1973. Formation of pore-structure. Proc. Int. Sym. RILEM/IUPAC Prague. 3B:5-35.

Shakoor,A., West,T.R. and C.F. Scholer. 1982. Physical characteristics of some Indian Argilloceous car-

bonates regarding their freeze-thaw resistance in concrete. Bull. Assoc. Eng. Geol. 19(4):371-384.

Stark,D. 1976. Characteristics and utilization of coarse aggregates associated with D-cracking (RDO47.01P). Portland Cement Association. Reprinted from Living With Marginal Aggregates. STP 597 ASTM Philadelphia, Pa.,1976:45-58

Talash,A.W. and P.B. Crawford. 1965. Rock properties computed from random pore-size distribution. Jr. Sed. Pet. 35(4):917-921.

Terrell,A.C. 1973. Recent advances in automatic image analysis. Proc. Int. Sym. RILEM/IUPAC Prague. 6C:506-515.

Thompson,S.R., Olsen,M.P.J. and B.J. Dempsey 1980. Synthesis report,D-cracking in Portland cement concrete pavements. Trans. Eng. Ser. No. 29. U. of Illinois.

Traylor,M.L. 1982. Efforts to eliminate D-cracking in Illinois. Trans. Res. Rec. 853:9-14.

Timur,A., Hempkins,W.B. and R.M. Weinbradt. 1971. Scanning electron microscope study of pore systems in rocks. Jr. Geophysical Research. 76(20):4932-4948.

Valenta,O. 1973. Main properties of the pore systems of non-metallic structural materials, their significance and experimental determination. Proc. Int. Sym. RILEM/IUPAC Prague. 2E:75-101.

Wardlaw,N.C. 1976. Pore geometry of carbonate rocks as revealed by pore casts and capillary pressure. Bull. Am. Ass. Pet. Geol. 60(2):245-257.

Wardlaw,N.C and R.P. Taylor. 1976. Mercury capillary pressure curves and the interpretation of pore structure and capillary behavoir in resivoir rocks. Bulletin of Canadian Petroleum Geology. 24(2):225-262.

Wardlaw,N.C. 1981. Mercury porosimetry and the interpretation of pore geometry in sedimentary rocks and artificial models. Powder Technology. 29:127-143.

Zagar,L. 1973. Methods of determination of pore-structure permeability and diffusion. Proc. Int. Sym. RILEM/IUPAC Prague. 6C:249-277.

## BIBLIOGRAPHY


Beaudoin,J.J. 1979. Porositiy measurement of some hydrated cementitous systems by high pressure mercury intrusion-microstructural limitations. Cement and Concrete Research. 9,6:771-781.

Dinkle,R.E. 1966. Freezing resistance in mortar related to pore properties of rock particles. MSc Thesis,U. of Maryland.

Dolar-Mantuani, L. 1966. Petrographic examination of natural concrete aggregates. Hwy. Res. Rec. No.120:7-17.

Dubinin,M.M. 1973. Methods of determination of pore-structure,adsorption methods. Proc. Int. Sym. RILEM/IUPAC Prague. 4F:140-149.

Fagerlund,G. 1973. Pore-structure and frost resistence. Proc. Int. Sym. RILEM/IUPAC Prague. 4F:67-87.

Globus,A.M. and B.M. Mogilevsky. 1969. Thermal transfer of liquid in porous media. Hwy. Res. board Spec. Rep. 103:39-50.

Halverson,A.D. 1982. Recycling Portland cement concrete pavement. Trans. Res. Rec. 853:14-17.

Havens,J.H. and R.C. Deen. 1977. Possible explanation of concrete Pop-Outs. Trans. Res. Rec. 651:16-24.

Huang,J.,Sherwood,W.C. and N. Wakao. 1966. Determination of bmean pore radii in mineral aggregates using permeability measurement. Hwy. Res. Board Spec. Report. No 90:219-233.

Hudec,P.P. 1980. Durability of carbonate rocks as a function of their thermal expansion,water sorption and minerology. ASTM Spec. Tec. Pub. 697:497-508.

Koh,Y. and E. Kamada. 1973. The influence of pore-structure of concrete made with absorbtive aggregates on the frost durability of concrete. Proc. Int. Sym. RILEM/IUPAC Prague. 2F:45-62.

Koplik J., C. Lin and M. Vermette. 1984. Conductivity and permeability from microgeometry. J. Appl. Phys. 56(11):3127-3131.

Larson,T. and P. Cady. 1969. Identification of frost-susceptible particles in concrete aggregates. Hwy. Res. Board NCHRP report 66.

Lin C. and M.H. Cohen. 1982. Quantitative methods for microgeometry modeling. J. Appl. Phys. 53(6):4152-4165.

Lin C. 1982. Microgeometry I: Autocorrelation and rock microstructure. Mathematical Geology. Vol. 14 No. 4:343-360.

Lin C. 1982. Microgeometry II: Testing for homogeneity in Berra Sandstone. Mathematical Geology. Vol. 14 No. 4:361-370.

Lin C. 1982. Measurement of sphere contacts in a sectioning plane. Mathematical Geology. Vol. 14 No. 5:501-508.

Lin C. 1983. Shape and texture from serial contours. Mathematical Geology Vol. 15 No. 5:617-632.

Litvan,G.G. 1980. Freeze-thaw durability of porous building materials. ASTM Spec. Tech. Publ. 691:455-463.

Longman,M.W. and P.A. Mench. 1978. Diagenesis of cretaceous limestones in the Edwards Aquifer System south-central Texas:A scanning electron microscope theory. Sedimentary Geology. 21:241-276.

Longman,M.W. 1980. Carbonate diagenetic textures from nearsurface diagenetic environments. AAPG Bull. 16,4:461-487.

MacInnis,C. and J.J. Beaudoin. 1973. Pore-structure and frost durability. Proc. Int. Sym. RILEM/IUPAC Prague. 2F:3-15.

Marks,V.J. and W. Dubberke. 1982. Durability ao concrete and the Iowa Pore Index Test. Trans. Res. Rec. 853:25-31.

Meininger,R.C. 1964. Influence of aggregate pore properties on the resistance of concrete to freezing damage. MSc thesis,U of Maryland.

Murphy C.P., P. Bullock and R.H. Turner. 1977. The measurement and characterisation of voids in soil

thin sections by image analysis. Part I. Principles and Techniques. Jr. Soil Science 28:498-508.

Murphy C.P., P. Bullock and K.J. Biswell. 1977. The measurement and characterisation of voids in soil thin sections by image analysis. Part II. Applications. Jr. Soil Science 28:509-518.

Mysyk,W.K. and R.J. Edwards. 1984. Petrological analysis of concrete aggregates in Apron 1 at Winnipeg International Airport, Winnipeg, Manitoba. Tansport Canada Report.

Olsen,M.P.J, Janssen,D.J. and B.J. Dempsey. 1983. Final report,D-cracking in Portlant cement concrete pavements. Trans. Eng. Ser. No. 37. U. of Illinois.

Olsen,M.P.J. 1984. Mathmatical modeling of the freezing processing in concrete and aggregates. Cem. Concrete Res. 14,1:113-122.

Ondracek,G. 1973. Mean stereometric factors and properties of porous materials. Proc. Int. Sym. RILEM/IUPAC Prague. 6======?.

Paxton,J.J. 1982. Ohio aggregate and concrete testing to determine D-cracking susceptibility. Trans Res. Rec. 853:20-24.

Pimenov,V.V., Vladimir,B. and A. Angelina. 1973. structure of pores and ice formation processes in concrete. Proc. Int. Sym. RILEM/IUPAC Prague. 4F:89-98.

Podvalny,A.M. and A.M. Prozenko. 1973. An investigation of the permeability of porous bodies on a mathematical model. Proc. Int. Sym. RILEM/IUPAC Prague. 3A:13-31.

Portland Cement Association 1979. Design and control of concrete mixtures. Eng. Bull.

Powers,J.C. 1955. Basic considerations pertaining to freezing and thawing tests. Proc. ASTM. 55:1132-1155.

Reilly,R.J. 1962. The effect of moisture content and distribution on the durability of concretes containing various coarse aggregates. MSc Thesis, U. of Maryland.

Rink,M. 1973. Investigations on the pore geometry of sedimentary rocks by an image analysis procedure for digital computers. Z. Geophys. 39(6):989-1005.

Scheidegger,A.E. 1973. Models and geometry of pore-structure. Proc. Int. Sym. RILEM/IUPAC Prague. 3A:3-12.

Schopper,J.R. 1973. A statistical network model and theory of porous media. Proc. Int. Sym. RILEM/IUPAC Prague. 1A:53-71.

Straley C. 1983. A brominated epoxy embedding system. Powder Technology No. 35:259-261.

Taylor,R.P. and N.C. Wardlaw. 1975. Increased precision of porosity measurements using a modified Ruska Universal Porometer. Jr. Can. Pet. Tech. 14:33-37.

Venecanin,S.D. 1977. Influence of temperature on detereioration of concrete in the Middle East. Concrete. 11(8):31-32.

Verbeck,G. and R. Landgren. 1960. Influence of physical characteristics of aggregates on frost resistance of concrete. ASTM Proceedings. 60:1063-1079.

Walker,R.D. 1965. Idendification of aggregates causing poor concrete performance when frozen. Interim Report NCHRP No. 12.

Walker,R.D. 1966. Identification of coarse aggregates that undergo destructive volume changes when frozen in concrete. Hwy. Res. Rec. 120:1-6.

Walker,R.D. and T. Hsich. 1968. Relationship between aggregate pore characteristics and durability of concrete exposed to freezing and thawing. Hwy. Res. Rec. 226:41-49.

Wardlaw,N.C. 1979. Pore systems in carbonate rocks and their influence on hydrocarbon recovery efficiency. Short Course on Carbonate Porosity. AAPG Continuing Education Course Note Series #11.

Winslow,D.N, Lindgren,M.K. and W.L. Dolch. 1982. Relationship between pavement D-cracking and coarse aggregate pore structure. Trans. Res. Rec. 853:17-19.

# Appendix F

## GLOSSARY OF TERMS

## Glossary of Terms

bitplane image

Computer printout of the detectected image obtained using image analysis procedures.

capillary

The interconnecting channels of the pore structure of microscopic size.

capillary suction

Stress exerted on a wetting fluid such as water ( < 90 ) which is inversely proportional to the radius of the pore.

capillary depression

Reverse of capillary suction for a non-wetting fluid ( > 90 ). Mercury (Hg) most common example.

diagenesis

All chemical , physical and biological changes and modifications undergone by a sediment after its initial deposition, and during and after lithification, exclusive of weathering and metamorphism.

pixel

Commonly referred to as picture point. A pixel is an element of which a computer image is comprised. The LEITZ TAS PLUS digitizing screen is comprised of a 512X512 pixel array.

pore segment

Two-dimensional void space descriminated in the microscopic detection of pore casts.

erosion

The removal of a layer of pixels from a binary image of a pore segment.

dilation

The opposite of erosion: adds 1 layer of pixels to the binary image of the pore segment.

E-D cycle

One erosion dilation cycle.

effective porosity

Interconnected void space (porosity).

Image Analysis

Computer techniques for the aquisition, segmentation and analysis of 2-dimensional images.

Petrographic Image Analysis (PIA)

Geological computer image analysis techniques used for porosity evaluation.

pore cast

Epoxy resin replica of the pore space impregnated by a blue dyed resin. Ground and pollished to form a 2-dimensional image of the rock porosity.

porosity

(Volume of void space/total volume) or (area void space/total area).

pore coordination

Connectivity of pores related to the number of connected channels.

pore

Wider part of pore network.

pore throat

Narrower part of pore network.

pore size

Portion of pore that represents the simplest geometry of a pore segment obtained using erosion-dilation algorithm.

pore roughness

Portion of pore represented by the complex irregularities of a given pore segment obtained using the erosion-dilation algorithm.

pore complex spectra

Frequency distributions that represent a method for the characterization of the geometry of a given pore complex. These spectra partition the total porosity into pore and roughness porosity.